entropy

MDPI

Article

Nonlinear Relaxation Phenomena in Metastable Condensed Matter Systems

Bernardo Spagnolo [1,2,3,*], Claudio Guarcello [4,5,3], Luca Magazzù [6], Angelo Carollo [1,3], Dominique Persano Adorno [1] and Davide Valenti [1]

1 Dipartimento di Fisica e Chimica, Interdisciplinary Theoretical Physics Group, Università di Palermo and CNISM, Unità di Palermo, Viale delle Scienze, Edificio 18, I-90128 Palermo, Italy; angelo.carollo@unipa.it (A.C.); dominique.persanoadorno@unipa.it (D.P.A.); davide.valenti@unipa.it (D.V.)
2 Istituto Nazionale di Fisica Nucleare, Sezione di Catania, Catania, Italy
3 Radiophysics Department, Lobachevsky State University of Nizhni Novgorod, Nizhni Novgorod, Russia
4 SPIN-CNR, Via Dodecaneso 33, I-16146 Genova, Italy; claudio.guarcello@unipa.it
5 NEST, Istituto Nanoscienze-CNR and Scuola Normale Superiore, Piazza S. Silvestro 12, I-56127 Pisa, Italy
6 Institute of Physics, University of Augsburg, Universitätsstrasse 1, D-86135 Augsburg, Germany; luca.magazzu@unipa.it
* Correspondence: bernardo.spagnolo@unipa.it; Tel.: +39-091-238-99059

Academic Editor: Kevin H. Knuth
Received: 12 November 2016; Accepted: 25 December 2016; Published: 31 December 2016

Abstract: Nonlinear relaxation phenomena in three different systems of condensed matter are investigated. (i) First, the phase dynamics in Josephson junctions is analyzed. Specifically, a superconductor-graphene-superconductor (SGS) system exhibits quantum metastable states, and the average escape time from these metastable states in the presence of Gaussian and correlated fluctuations is calculated, accounting for variations in the the noise source intensity and the bias frequency. Moreover, the transient dynamics of a long-overlap Josephson junction (JJ) subject to thermal fluctuations and non-Gaussian noise sources is investigated. Noise induced phenomena are observed, such as the noise enhanced stability and the stochastic resonant activation. (ii) Second, the electron spin relaxation process in a n-type GaAs bulk driven by a fluctuating electric field is investigated. In particular, by using a Monte Carlo approach, we study the influence of a random telegraph noise on the spin polarized transport. Our findings show the possibility to raise the spin relaxation length by increasing the amplitude of the external fluctuations. Moreover, we find that, crucially, depending on the value of the external field strength, the electron spin depolarization length versus the noise correlation time increases up to a plateau. (iii) Finally, the stabilization of quantum metastable states by dissipation is presented. Normally, quantum fluctuations enhance the escape from metastable states in the presence of dissipation. We show that dissipation can enhance the stability of a quantum metastable system, consisting of a particle moving in a strongly asymmetric double well potential, interacting with a thermal bath. We find that the escape time from the metastable region has a nonmonotonic behavior versus the system- bath coupling and the temperature, producing a stabilizing effect.

Keywords: metastability; nonequilibrium statistical mechanics and nonlinear relaxation time; noise enhanced stability; Josephson junction; spin polarized transport in semiconductors; open quantum systems; quantum noise enhanced stability

1. Introduction

Nonlinear relaxation phenomena in the presence of metastable states are ubiquitous phenomena in condensed matter systems. Specifically, metastability is a universal phenomenon in many

natural systems, ranging from physics to cosmology, chemistry, biology and ecology [1–4]. Indeed, metastability is an active research field in statistical physics [5–11]. Understanding metastability is a fundamental issue to understand and describe the dynamical behavior of many natural systems. In fact, metastability is relevant in the dynamical behavior of complex systems, such as spin glasses and glasses, and its relevance depends on the number of metastable states, their local stability and related basin of attraction in the presence of thermal or external fluctuations [12]. It is the time scale of the basin of attraction around the investigated stable point of the system that defines the stability and metastability of state under consideration. Metastability is a signature of a first order phase transition, often characterized by a long-living metastable state, whose dynamics is typical of out-of-equilibrium systems [5,12,13]. Specifically, metastable states in complex systems are characterized by different time scales, the fast ones describing the dynamics inside the metastable region and the slow ones describing the dynamics between different metastable states, and often it is interesting to find long-living metastable states [5,6,13]. In particular, the stability of a metastable state can be enhanced by Gaussian and non-Gaussian noise sources [14–17].

Moreover, in recent years, several theoretical investigations have focused on the positive effects of the noise on nonlinear systems, showing that, under suitable conditions, the addition of external fluctuations to intrinsically noisy systems may induce an enahncement of the dynamical stability of the system, resulting in a less noisy response [18–28]. This counterintuitive effect has been found in different physical areas, ranging from the generation of spin currents [29], aggregation kinetics of Brownian particles [30,31], chemical reaction system [32], translocation dynamics of polymers [33–35], ultra-fast magnetization dynamics of magnetic spin systems [36,37], dynamic electron response in zinc-blende semiconductor crystals [38–43], noise redistribution in quasi 2D Silicon Mos inversion layers [44], to interdisciplinary physical models [45–52].

Several theoretical studies have shown that the average escape time from metastable states in the presence of fluctuating and static potentials is characterized by nonmonotonical behavior with respect to the noise intensity [14,23,53–67]. This resonance-like behavior, called noise enhanced stability (NES), is in contrast with the monotonic behavior predicted by Kramers theory [68,69]: the stability of metastable or unstable states is in fact enhanced by the noise with the average lifetime resulting larger than the deterministic one. For a classical Brownian particle in a cubic potential, the mean first passage time (MFPT) as a function of the noise intensity, D, is characterized by a maximum when the particle is placed initially outside the metastable well, in a certain region on the right of the potential maximum, that is in a nonequilibrium position. For very low noise intensities, in the limit $D \to 0$, the MFPT diverges as a consequence of the trapping of the Brownian particle in the potential well [54,55]. Increasing the value of D, the particle can escape out more easily and the MFPT decreases. As the noise intensity reaches a value $D \approx \Delta U$, with ΔU the potential barrier height, the escape process of the Brownian particle is slowed down, due to the fact that the probability to reenter the well is increased. At higher noise intensities, one recovers a monotonic decreasing behavior of the MFPT. In summary, the behavior of the MFPT vs D goes with continuity from a monotonic divergent behavior to a nonmonotonic finite behavior (typical NES effect), passing through a nonmonotonic divergent behavior with a minimum and a maximum [55]. Very recently, the noise stabilizing effects were also observed in quantum systems with asymmetric bistable potentials [7].

In this paper we shortly review three noise induced phenomena characterizing the nonlinear relaxation of short and long Josephson junctions (JJ), spin transport in n-type GaAs bulk, and populations of spatially localized states in a strongly asymmetric quantum bistable system. Specifically, the three induced effects investigated are the noise enhanced stability, the stochastic resonant activation and the noise-induced coherence of electron spin.

JJs are typical out-of-equilibrium systems characterized by tilted or switching periodic potentials [70,71]. Recently, JJs as superconducting quantum bits [72–74], nanoscale superconducting quantum interference devices [75] for detecting weak flux changes, and threshold noise detectors has attracted the interest of researchers [76–78]. The dynamics of these devices is affected by

environmental perturbations and, in particular, by random fluctuations responsible for decoherence phenomena. The effects of both thermal and non-thermal random fluctuations on the behavior of normal and graphene-based JJs were recently investigated [17,79–81].

Semiconductors spintronics offers a fruitful direction for scientific research towards the development of electron spin-devices performing logic operations, communication and storage. The main focus is to obtain long spin relaxation times or long spin diffusion lengths. In fact, electron spin states depolarize by scattering from imperfections or phonons. Indeed, during the transport of the spin system, the spin of conduction electrons decays over time due to the combined effect of spin-orbit coupling and momentum scattering. Moreover, the electron-electron dynamic collisions and the static fluctuations in the density of dopant ions give rise to a randomness of the spin-orbit coupling. A question naturally rises: external fluctuations could play a positive role in the process of spin relaxation in semiconductors? Despite some previous investigations [82–84], the possibility of using the external fluctuations, added to the driving electric field, to positively affect the spin decoherence process is still an open question.

A classical metastable state decays to a more stable configuration by thermally surmounting a potential barrier in the presence of an external influence on the system, such as the one exerted by a noise source. On the other hand, the decay of a quantum metastable state occurs also by means of the tunneling mechanism, and in isolated systems, where the tunneling rate is determined by the geometry of the potential barrier. In the presence of a dissipative environment, the time scale of the decay is dictated by the temperature of the environment and by the details of its coupling with the quantum system, other than by the potential profile.

Real-time path integral calculations on the tunneling dynamics started with the seminal work by Caldeira and Leggett [85] on the tunneling rate in superconducting devices. Within a N-level approximation of the open quantum system, the real-time approach allows for capturing the dynamics of the particle in terms of populations of spatially localized states in bistable potentials [86,87].

An increase of the decay time from the metastable state vs. the noise strength, with a maximum at an optimal value of the noise, takes the name of noise enhanced stability (NES). Such phenomenon, in a classical context, has been established both experimentally and theoretically [14,53,54].

Motivated by the classical case, we investigate the presence of NES in quantum metastable systems at strong dissipation. We do this by means of the real-time path integral approach and by varying the coupling strength and the temperature of the environment. The analysis relies on a initial condition substantially different from the quasi-equilibrium state inside the metastable well, which is considered in previous studies on quantum decay rates [88,89]. The preparation is indeed assumed to be of the kind used for classical system where NES is predicted, namely the particle initially in a nonequilibrium position between the top of the barrier and the so-called exit point of the potential [86].

The paper is organized as follows. In the next section the transient dynamics of short and long JJ is analyzed. In section 3 the nonlinear relaxation process of an electron spin system and its noise-induced coherence are investigated. Finally in section 4 the transient dynamics of a quantum metastable system in the presence of strong Ohmic dissipation is presented. In the last section we draw the conclusions.

2. Short and Long JJ

A Josephson junction (JJ) is a superconducting device composed by two superconductors separated by a thin layer of non-superconducting material. In this mesoscopic device, which can be in a resistive or superconducting state, the current and the voltage across the junction are related to the microscopic order parameter φ, that is the phase difference between the wave functions describing the ground state in the two superconductors [17,79,90,91]. Recently, the effects of both thermal and non-Gaussian fluctuations on the dynamics of JJs have been the focus of increasing

investigations [16,17,92–95]. Indeed, the statistical analysis of the switching from the metastable superconducting state to the resistive one of a JJ has been used as a theoretical tool to detect signals with unknown statistics [77,78,96].

- Short Graphene JJ

Recently, Josephson devices with a graphene sheet as interlayer has attracted an increasing scientific interest [97,98]. Experimental evidence of superconducting states in graphene, with coherent propagation of Cooper pairs, has been recently found [99–101]. Moreover, noise effects in the dynamical behavior of graphene JJs have been analyzed from experimental and theoretical point of view [97,100,102–104]. In this section we study the transient dynamics of an underdamped superconductor−graphene−superconductor (SGS) junction, as the simultaneous action of an external driving force, oscillating with frequency ω, and a stochastic signal, which represents a random force of intensity γ, is taken into account. Specifically, we analyze the mean lifetime of the superconductive state of the device by varying the frequency ω and the noise intensity γ.

- Long JJ

In condensed matter physics the defects inside a solid state lattice can give rise to fluctuations of electrical resistance and diffusion, which can be described by a random telegraph noise [91,105,106]. In this section we study the effects of a source of dichotomous random telegraph noise (dRTN) on a long JJ (LJJ), driven by both a constant and an oscillating bias current. Specifically, we investigate the mean switching time (MST), namely, the average time the junction takes to switch from the superconducting state to the resistive regime, as a function of several parameters of system and noise source. The phase dynamics of a LJJ, analyzed within the sine-Gordon (SG) formalism [17,81,90], is characterized by a peculiar excitation, called soliton or kink [107,108], related to the penetration of a magnetic flux quantum, i.e., fluxons [109,110], generated by a supercurrent circulating around it.

2.1. Short Graphene JJ—Model

According to the resistively and capacitively shunted junction (RCSJ) model [90] and including the environmental influence, the equation of motion for the order parameter φ in a short JJ reads

$$\frac{\partial^2\varphi}{\partial t^2} + \beta_J \frac{\partial \varphi}{\partial t} = i_b(t) - i_\varphi(t) + i_f(t), \tag{1}$$

where $i_b(t)$ and $i_\varphi(t)$ are the bias and supercurrent, respectively, both normalized to the critical current of the junction I_c. The term $i_f(t)$, also normalized to I_c, represents the stochastic noise contribution. In Equation (1), $\beta_J = (\omega_{p_0} RC)^{-1}$ is the damping parameter and the time variable is normalized to the inverse of the zero-bias plasma frequency $\omega_{p_0} = \sqrt{2\pi I_c/(\Phi_0 C)}$. The dynamics of a short JJ can be viewed in terms of the motion of a "phase particle" with mass $m = C(\Phi_0/2\pi)^2$ rolling down along the washboard potential (WP).

The non-sinusoidal current-phase relation and the critical current for a short ballistic graphene JJ in the low temperature regime, i.e., $T \lesssim T_c/4$ (T_c being the critical temperature of the junction), can be written as [80,111,112]

$$i_\varphi(t) = \frac{I(\varphi)}{I_c} = \frac{2}{1.33}\cos\left(\frac{\varphi}{2}\right)\tanh^{-1}\left[\sin\left(\frac{\varphi}{2}\right)\right] \tag{2}$$

$$I_c = 1.33\frac{e\Delta_0}{\hbar}\frac{W}{\pi L}. \tag{3}$$

From Equation (2) a washboard-like potential can be also defined [80]. In Equation (3), W and L are the length of the superconductive plates and their separation, respectively, and Δ_0 is the superconductive excitation gap. According to the short junction regime, $L \ll W, \xi$ [111], where ξ is

the superconducting coherence length. The bias current is composed of a constant term, i_0, and an oscillating part, containing a phase term ϕ_0,

$$i_b(t) = i_0 + A \sin(\omega t + \phi_0). \tag{4}$$

Specifically, in every numerical realization a value of ϕ_0 is randomly drawn within $[0, 2\pi]$. Accordingly, the initial slopes of the WP are randomly distributed in the range $[i_0 - A, i_0 + A]$, whereas the mean slope is still equal to i_0. In Equation (4), the frequency ω is normalized to ω_{p_0}.

The junction leaves the superconductive regime when the phase particle, initially placed in the bottom of a potential minimum, reaches one of the nearest maxima, in correspondence of which absorbing barriers are placed. Recording for each numerical realization the escape time, namely, the time required to reach a barrier, the MFPT for a large enough number N of realizations is calculated.

The stochastic normalized current $i_f(t)$ is characterized by the well-known statistical properties of a Gaussian random process

$$\left\langle i_f(t) \right\rangle = 0 \qquad \left\langle i_f(t) i_f(t+t') \right\rangle = 2\gamma(T)\delta(t'), \tag{5}$$

where normalized units for the current and the time are used, and the dimensionless amplitude $\gamma(T)$ reads

$$\gamma(T) = \frac{\omega_{p_0}}{\omega_c} \frac{2e}{\hbar} \frac{kT}{I_c}. \tag{6}$$

The stochastic dynamics is analyzed by integration within the Ito scheme of Equation (1) with a finite difference method. The time step and the integration time are $\Delta t = 10^{-3}$ and $t_{max} = 100$, respectively.

2.1.1. Short Graphene JJ—Results

The behavior of the lifetime of the superconductive state, τ, that is the MFPT, as a function of the noise intensity γ and the driving frequency ω, for $i_0 = 0.1$, is shown in the panels of Figure 1. In particular, the escape times show maxima for suitable values of γ, namely, the NES effect, while minima are observed for certain values of the driving frequency, i.e., the resonant activation (RA) effect. More in detail, Figure 1 shows the results for $i_0 = 0.1$ in the absence of the phase ϕ_0 in the oscillating bias (i.e., $\phi_0 = 0$), while the case of randomly distributed phase ϕ_0 in $[0, 2\pi]$ is shown in Figure 1. It is noteworthy that for frequencies higher than the plasma frequency, namely, $\omega > 1$, at low noise intensities a trapping phenomenon occurs [17]. A threshold frequency ω_{thr} exists such that for $\omega > \omega_{thr}$ the phase particle is trapped between two successive minima of the potential profile, and cannot move to the next WP valley. Accordingly, the MFPT diverges in the limit $\gamma \to 0$.

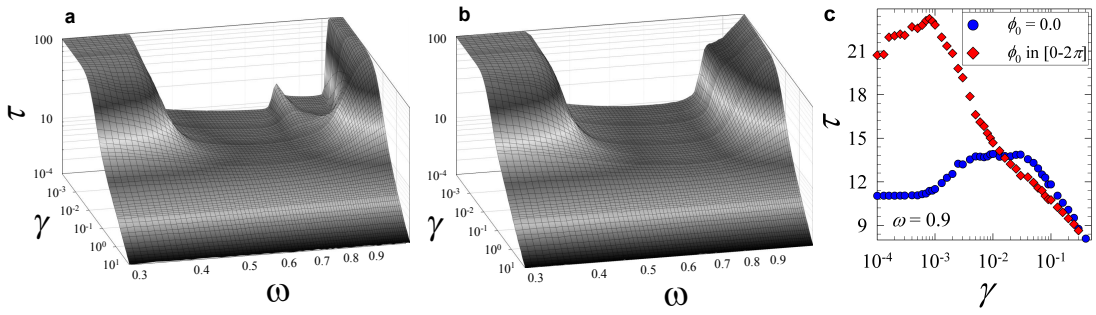

Figure 1. (**a**) and (**b**), mean first passage times (MFPTs) τ as a function of ω and γ, for both $\phi_0 = 0$ and a randomly distributed ϕ_0 in $[0 - 2\pi]$, respectively; (**c**) MFPTs τ as a function of γ for $\omega = 0.9$, for both $\phi_0 = 0$ and a randomly distributed ϕ_0 in $[0 - 2\pi]$. For (**a**)–(**c**), the other parameters are $i_0 = 0.1$, $A = 0.7$, $\beta_J = 0.1$, and $N = 10^4$.

In Figure 1a two different kinds of RA can be clearly distinguished. The dynamic resonant activation (DRA), which occurs for low noise intensities as the external driving frequency is close to the natural characteristic frequency of the system, that is the plasma frequency of the JJ [80,113–115], and the stochastic resonant activation (SRA), which occurs for driving frequencies close to the inverse of the average escape time at the minimum, i.e., the mean escape time over the potential barrier in the lowest configuration [78,80,116,117]. For $i_0 = 0.1$, the DRA effect is characterized by two minima, which appearance is related to as many escape resonance phenomena, one through the right potential barrier and the other through the left one. This double-minima effect is highly sensitive to the initial potential slope [80], so that it is expected to vanish as the random phase ϕ_0 is included into the model, see Figure 1b. In this case, independently of the noise amplitude, τ values show a smoothed large "dip" (see Figure 1b), in the bottom of which also the NES effect seems weakened. Conversely, NES persists for frequency still within the dip, but far away from its bottom (see Figure 1c). For a better insight of the NES phenomenon, we observe the probability density functions (PDFs) of the normalized switching times, $P(t/\mathrm{T}_p)$, calculated setting $\omega = 0.44$ and $i_0 = 0.1$, for $\phi_0 = 0$ and $\phi_0 \in [0 - 2\pi]$, see Figure 2. For $\phi_0 = 0$, close to the NES maximum the PDFs are composed by long regular sequences of equidistant sharp peaks with exponentially decreasing amplitude [80,118], see results for $\gamma = 0.01$ in Figure 2a. More generally, for $\gamma < 1$, the PDFs are distributions of a series of two distinct asymmetric peaks per driving period T_p, where the peaks placed within the odd (even) multiples of the half driving period represent escape events through the right (left) potential barrier. Increasing the noise intensity, $\gamma > 1$, the peaks tend to become lower and broader, and they eventually merge into a larger distribution.

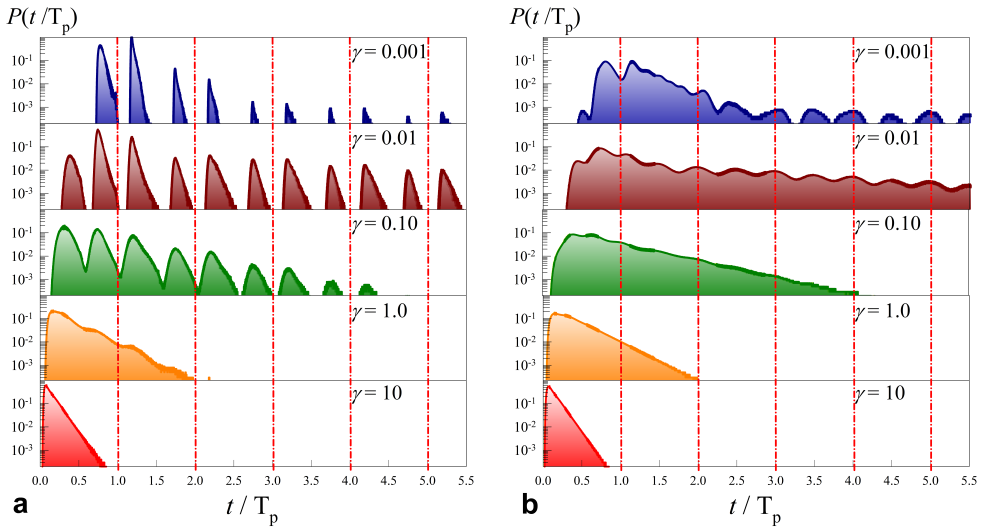

Figure 2. (Color online) Probability density functions (PDFs) P as a function of the normalized time t/T_p (T_p is the driving period), varying γ, for (**a**) both $\phi_0 = 0$ and (**b**) a randomly distributed ϕ_0 in $[0 - 2\pi]$. Every picture is obtained for $A = 0.7$, $i_0 = 0.1$, $\beta_J = 0.1$, and $\omega = 0.44$. The amounts of numerical realizations performed to build these PDFs are (**a**) $N = 10^7$ and (**b**) $N = 10^8$.

When a non-zero random phase is included into the oscillating bias, the PDFs behavior, interestingly, change, see Figure 2b. The PDF peaks tend to enlarge, up to coalesce. In spite of the random distributed driving phase ϕ_0, for $\gamma = 0.01$ and 0.001 (at least for $t > 2\mathrm{T}_p$) we note that the peaks are exactly located for $t = [(k+1)/2]\mathrm{T}_p$, with $k = 1, 2, 3, \ldots$. Accordingly, the resonant escapes mainly occur as the WP slope assumes the mean value i_0. For $\gamma = 0.1$ the shape of individual peaks is no longer distinguishable, so that a large distribution, extending approximatively up to $t \sim 4\mathrm{T}_p$, is obtained. Similarly, for $\gamma = 1.0$ and 10, single-peak PDFs result, extending up to $t \sim 2\mathrm{T}_p$ and $t \sim \mathrm{T}_p$, respectively.

2.2. Long JJ—The model

The electrodynamics of a long JJ (LJJ) can be analyzed looking at the time evolution of the order parameter φ, which is ruled by the sine-Gordon equation, that, in normalized units, is expressed by [90]

$$\beta_c \frac{\partial^2 \varphi}{\partial t^2} + \frac{\partial \varphi}{\partial t} - \frac{\partial^2 \varphi}{\partial x^2} = i_b(t) - \sin(\varphi) + i_{\mathrm{DN}}(t), \tag{7}$$

with boundary conditions $\frac{\partial \varphi(0,t)}{\partial x} = \frac{\partial \varphi(L,t)}{\partial x} = 0$, L being the junction length (in units of the Josephson penetration depth λ_J [90]). The space x and the time t are normalized to λ_J and to the inverse of the characteristic frequency $\omega_c = 2\pi I_c R/\Phi_0$ [90], respectively. The coefficient $\beta_c = \omega_c RC$ is the Stewart-McCumber parameter [90] (R and C are the normal resistance and the capacitance of the junction, respectively) and is set to $\beta_c = 0.01$ (overdamped condition) in the numerical calculations.

The bias current $i_b(t)$ is normalized to the critical current of the junction. The effects of a dichotomous noise source is taken into account by the term $i_{\mathrm{DN}}(t)$. For the sake of understanding the exclusive effect of the dRTN source $i_{\mathrm{DN}}(t)$ on the LJJ response, a thermal noise source, which effects were formerly extensively explored in the LJJ context [17,81,119–123], is ignored in this model. A LJJ can be depicted as a string lying along a potential, the washboard potential (WP) $U(\varphi, x, t)$, given by

$$U(\varphi, x, t) = 1 - \cos[\varphi(x,t)] - i_b(t)\, \varphi(x,t). \tag{8}$$

The WP is formed by a sequence of minima, namely, the metastable states of the junction. The string is initially at rest at the bottom of a washboard valley, that is $\varphi(x,0) = \arcsin(i_0)\, \forall x : 0 \leq x \leq L$. The bias current $i_b(t)$ gives the slope of this potential and is the sum of a constant term i_0 and an oscillating component

$$i_b(t) = i_0 + A\, \sin(\omega t), \tag{9}$$

where the frequency ω is normalized to ω_c and $A = 0.7$. When $i_b \geq 1$ the potential barriers ΔU between consecutive minima of the potential vanish and the metastable states are removed.

The stochastic current $i_{\mathrm{DN}}(x,t)$, representing the dRTN signal, reads

$$i_{\mathrm{DN}}(x,t) = \gamma\, \beta(t), \tag{10}$$

where γ is the normalized noise amplitude. The parameter $\beta(t)$ is a dichotomous stochastic process jumping between two values, β_{up} and β_{down}, with a rate:

$$\gamma_{\mathrm{DN}}(t) = \begin{cases} 0, & \Delta t_r \leq \tau_d \\ \gamma_0 \left(1 + A_{\mathrm{DN}} \left|\cos\left(\omega_{\mathrm{DN}} t\right)\right|\right), & \Delta t_r > \tau_d. \end{cases} \tag{11}$$

Here, Δt_r is the random time interval between two consecutive switches, and τ_d is the delay between two jumps, that is the time interval after a switch, before another jump can occur. A similar approach to model the dichotomous noise source was previously implemented and used in other contexts, from generalized Lotka-Volterra systems [124–127] to electron transport dynamics in GaAs samples [41]. Equation (7) is numerically solved within the Ito scheme by setting $\Delta t = \Delta x = 0.05$. The MST τ is a nonlinear relaxation time (NLRT) [14,17,81,91] and represents the mean value of the permanence times of the phase φ within the first valley, that is $\varphi \in [\varphi^L_{Max}\ ,\ \varphi^R_{Max}]$. The thresholds φ^L_{Max} and φ^R_{Max} are, respectively, the positions of the left and right maxima which surround the minimum chosen as initial condition. No absorbing barriers are set, so that during the entire observation time, t_{max}, all the temporary trapping events are taken into account to calculate τ. In the i-th realization for the j-th cell, the probability $P_{ij} = 1$ if $\varphi \in [\varphi^L_{Max}\ ,\ \varphi^R_{Max}]$ and zero otherwise. Summing $P_{ij}(t)$ over the

total number $N_c = L/\Delta x$ of cells and over the number N of realizations, the average probability that the entire string is in the superconducting state at time t is computed as

$$\overline{P}(t) = \frac{1}{N\,N_c} \sum_{i=1}^{N} \sum_{j=1}^{N_c} P_{ij}(t). \tag{12}$$

The MST τ is therefore calculated as

$$\tau = \int_0^{t_{max}} \overline{P}(t) dt. \tag{13}$$

2.2.1. Long JJ—Results

Here, we analyze the LJJ behavior and the emergence of noise-induced phenomena in the presence of a dRTN source, when the driving frequency is ranged in $\omega \in]10^{-3} - 10]$.

First of all, we note that the dRTN signal of Equation (10), applied to the junction together with a bias current, can hinder or support the switching dynamics from the superconducting state. In particular, a noise contribution in the same direction with respect to the tilting imposed by a positive bias current assists the escape events. Conversely, a noise contribution of opposite sign to the bias current contrasts with the escape events and further confines the string within a potential minimum. Therefore, an initial value of the dichotomous noise of sign equal or opposite to the bias current can strongly affects the MST value. In fact, although the MST τ is a NLRT, the value of τ is highly influenced by the time the string requires for the first escape from the initial metastable state. Accordingly, by imposing $\beta(0) = \beta_{down}$ or $\beta(0) = \beta_{up}$ the evolution of the string and the value of τ can drastically change. Finally, to release the results from the initial condition of the dRTN, the value of $\beta(0)$ has to be randomly chosen among β_{down} and β_{up} in each numerical realizations. Therefore, to properly understand the mechanisms governing the phase dynamics, all these cases are explored. Specifically, Figure 3 show the results obtained as the initial value $\beta(0)$ of the dichotomous noise is set to β_{up}, β_{down}, and is randomly drawn, respectively.

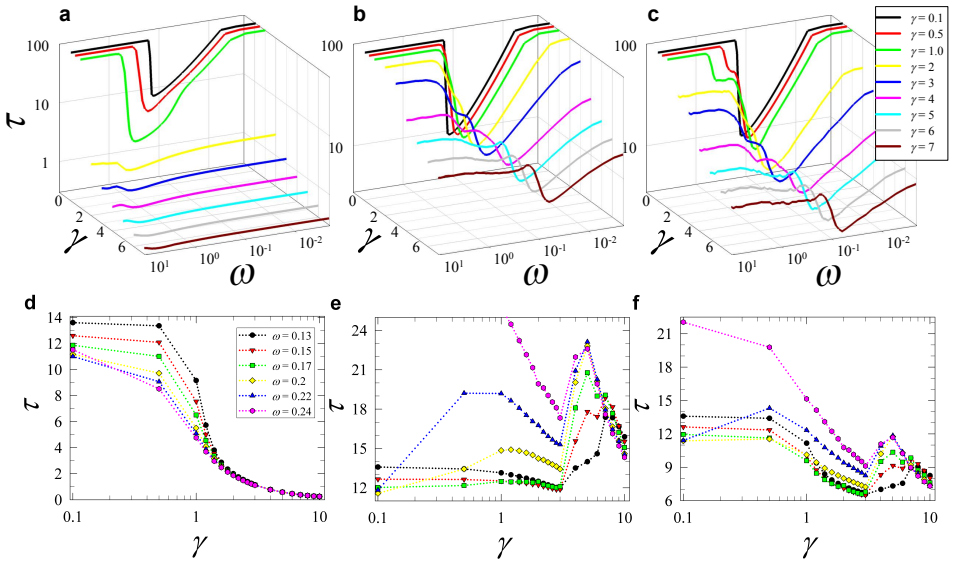

Figure 3. (Color online) (**a**)–(**c**), MST τ as a function of the driving frequency ω for several noise intensities with initial values of $\beta(t)$ set to up, down and randomly drawn (see (**a**)–(**c**), respectively); (**e**)–(**f**), MST τ as a function of the noise intensities γ for several driving frequency ω with initial values of $\beta(t)$ set to up, down and randomly drawn (see (**e**)–(**f**), respectively). For (**a**)–(**f**), the other parameters are $i_0 = 0.5$, $\tau_d = 3$, $A = 0.7$, $\beta_c = 0.01$, and $N = 5000$. The legend in (**c**) refers also to (**a**) and (**b**), whereas legend in (**d**) refers also to (**e**) and (**f**).

The MST τ as a function of the driving frequency ω for several noise intensities γ, $i_0 = 0.5$, and $\tau_d = 3$, are shown in Figure 3. Moreover, the length is set to $L = 20$, it means a junction long enough to observe solitons formation along the string [17,81,91,120].

Almost all curves of Figure 3 clearly show the presence of resonant activation [14,17,80,81,91,116, 118,128–135], specifically *stochastic resonance activation* [17,78,80,117], a noise induced phenomenon whose signature is the appearance of a minimum in the curve of MST vs ω.

In Figure 3a, as γ increases we note that τ rapidly reduces and the SRA phenomenon tends to vanish, for the first dichotomous jump is concordant with the bias tilting and the junction rapidly switches from the metastable state. Moreover, the SRA minimum tends to shift towards higher frequencies. The curves for $\gamma = 0.1$ for both $\beta(0) = \beta_{up}$ and $\beta(0) = \beta_{down}$ superimpose, indicating that, for small noise intensities, the MST is independent from the sign of the first jump of the dRTN source. When the down initial condition $\beta(0) = \beta_{down}$ is set, the SRA phenomenon is observed in all curves shown in Figure 3b. In this case, the SRA minimum slightly shifts towards lower frequencies as the noise intensity enhances. Interestingly, for $\gamma \gtrsim 5$ a small maximum follows the SRA minima, indicating a confinement of the system within the initial metastable states, according which τ slightly increases.

The curves in Figure 3c were obtained by randomly choosing the initial condition $\beta(0)$ of the dichotomous noise and are clearly an average between the results obtained setting $\beta(0) = \beta_{down}$ and those obtained for $\beta(0) = \beta_{up}$. Accordingly, the SRA phenomenon is still evident in all the curves shown in this figure.

Figure 3 show the presence of NES effect as few values of the driving frequency are set. We note that, in the range of noise amplitudes taken into account, this noise-induced phenomenon clearly emerges for $\beta(0) = \beta_{down}$, with maxima located in $\gamma \sim 1$ (for $\omega = 0.2$ and 0.22) and $\gamma \sim 5$, and accordingly when the $\beta(0)$ is randomly chosen. For the initial value of the β parameter $\beta(0) = \beta_{up}$ and the range of frequencies investigated, as we see from Figure 3, the MSTs show monotonic decreasing behavior as a function of the noise intensity. This is due to the initial slope of the potential profile, the low frequency values of the driving bias current and the low value of the rate of the dichotomous noise. All these parameters contribute to speed up the escape process from the superconductive metastable state to the resistive one, giving rise to a monotonic behavior of the MST, according to previous results obtained for a piecewise linear potential subject to a dichotomous noise source [14].

3. Spin Polarised Transport

The possibility of developing spin-based electronic devices in which the binary information is encoded in the two spin-states "up" and "down" gave rise to a huge number of investigations on electron spin phenomena in semiconductor structures, built on the idea to control the spin relaxation by electric currents or gate voltages [136–142]. A number of such devices have already been proposed [137,139,143], and the search for phenomena which can lead to spin based devices is widespread [136–138,140,141,144,145]. However, a disadvantage of the use of spin degree of freedom is that the magnetic polarisation relaxes over distance and time during the transport because of spin-orbit interactions or scattering events, by causing that the coherence is ensured for a too short time to enable the entire execution of the necessary spin manipulations. For this reason, the investigation of the spin relaxation processes represents a crucial point in spintronic device design [137,138]. Previous studies of the electron spin relaxation process in GaAs bulks have shown that external fluctuations added to the driving static electric field can affect the spin decoherence process [79,82–84], being this effect critically dependent on the amplitude of both the applied electric field and the external fluctuations, as well as on the noise characteristic times.

In this section we focus on the influence on the electron spin depolarization length of a random telegraph (RT) source of fluctuations, externally added to the forcing field in n-doped GaAs crystals in both low electric field and high electric field (more intense of the Gunn's field) regimes.

3.1. The Model

There exists a variety of effects which can lead to relaxation and dephasing of spin polarizations in GaAs crystals. However, for delocalized electrons and under nondegenerate regime, the D'yakonov-Perel (DP) mechanism [146,147] is the dominant relaxation process in n-type III-V semiconductors [148]. The spin-orbit interaction couples the spin of conduction electrons to the electron momentum, which is randomised by scattering with phonons, impurities and other carriers. The spin-orbit coupling gives rise to a spin precession, while momentum scattering makes this precession randomly fluctuating, both in magnitude and orientation [137,138].

In a semiclassical formalism, in absence of an external magnetic field, the term of the Hamiltonian of an electron in the conduction band which takes into account the spin-orbit interaction, has the form

$$H_{SO} = \frac{\hbar}{2}\vec{\sigma}\cdot\vec{\Omega}(\vec{k}). \tag{14}$$

It represents the energy of electron spins precessing around an effective magnetic field

$$\vec{B} = \hbar\vec{\Omega}(\vec{k})/\mu_B g \tag{15}$$

with angular frequency $\vec{\Omega}$, which depends on the orientation of the electron momentum vector with respect to the crystal axes; μ_B is the Bohr magneton and g is the electron spin g-factor. Near the bottom of the Γ-valley, the precession vector (Dresselhaus term) is given by

$$\vec{\Omega}_\Gamma = \frac{\beta_\Gamma}{\hbar}[k_x(k_y^2 - k_z^2)\hat{x} + k_y(k_z^2 - k_x^2)\hat{y} + k_z(k_x^2 - k_y^2)\hat{z}]. \tag{16}$$

In the equivalent L-valleys located along the [111] crystallographic direction, the precession vector is [149]

$$\vec{\Omega}_L = \frac{\beta_L}{\sqrt{3}}[(k_y - k_z)\hat{x} + (k_z - k_x)\hat{y} + (k_x - k_y)\hat{z}]. \tag{17}$$

In Equations (16) and (17), k_i ($i = x, y, z$) are the components of the electron wave vector, β_Γ= 23.9 eV ·Å^3 [150], and β_L=0.26 eV Å·2/$\hbar$ [151], are the spin-orbit coupling coefficients. Since the quantum-mechanical description of the electron spin dynamics is equivalent to that of a classical momentum $\vec{S}$ experiencing the magnetic field $\vec{B}$, we describe the spin evolution by the classical equation of precession motion

$$\frac{d\vec{S}}{dt} = \vec{\Omega}\times\vec{S}. \tag{18}$$

The DP mechanism acts between two collision events and randomises spin phases since electrons precess with different frequencies depending on their momenta. In fact, the direction of the precession axis and the effective magnetic field $\vec{B}$ changes randomly and in a trajectory-dependent way. This effect leads the spin precession frequencies $\vec{\Omega}$ and their directions to vary in an inhomogeneous way within the electron spin ensemble. This spatial variation, called *inhomogeneous broadening*, is quantified by the average squared precession frequency $\langle\mid\vec{\Omega}(\vec{k})\mid^2\rangle$ [152]. This quantity, together with the correlation time of the random angular diffusion of spin precession vector τ_Ω, are the relevant variables in the D'yakonov-Perel's formula [146]

$$\tau = \frac{1}{\langle\mid\vec{\Omega}(\vec{k})\mid^2\rangle\tau_\Omega}. \tag{19}$$

By following Matthiessen's rule, $1/\tau_\Omega = 1/\tau_p + 1/\tau_p^{'}$, where τ_p is the momentum relaxation time and $\tau_p^{'}$ is the momentum redistribution time, related to the electron-electron (e-e) scattering mechanism. Although e-e interaction contributes to momentum redistribution, it does not directly

lead to momentum relaxation [153]. The spin relaxation time τ results inversely proportional to both the correlation time of the fluctuating spin precession vector τ_Ω and the inhomogeneous broadening $\langle \mid \vec{\Omega}(\vec{k}) \mid^2 \rangle$. That is, scattering events are spin-indipendent and do not lead to phase randomization during the collision itself, but help to establish the random-walk-like evolution of the phase, leading to motional narrowing, like in nuclear magnetic resonance [152].

3.2. Monte Carlo Approach and Noise Modelling

The electron transport dynamics is simulated by a semiclassical Monte Carlo algorithm, which takes into account all the possible scattering events of the hot electrons in the medium [154,155] and includes the precession equation of the spin polarisation vector for each free carrier [149,156,157]. The Monte Carlo algorithm has been implemented by using a Multiparticle Multivalley FORTRAN Code, following the procedure extensively described in [158]. The electron-electron (e-e) interaction is accounted for by using the screened Coulomb potential and the Born's approximation. The e-e scattering is treated as an interaction between only two particles, by using the Peschke's approach [159], as refined by Moško and Mošková [160,161]. The conduction bands of GaAs are represented by the Γ-valley and four equivalent L-valleys. The complete set of n-type GaAs parameters used in our calculations is listed in Table I of [158]. All simulations are carried out in a GaAs single crystal with a doping concentration n equal to 10^{21} m^{-3}. We assume that all donors are ionised and that the free electron concentration is equal to the doping concentration. An ensemble of 5×10^4 electrons is used to collect spin statistics. All physical quantities of interest are calculated after a transient time long enough to achieve the steady-state transport regime.

The spin relaxation simulation starts with all electrons of the ensemble in the Γ valley, initially polarised $(S(0) = 1)$ along the $\hat{x}$-axis of the crystal, at the injection plane $(x_0 = 0)$. In order to extract the characteristic time τ of the spin relaxation, the obtained trend of the spin dephasing is fitted by the following exponentially time decaying law

$$\langle S_x \rangle(t) = A \cdot \exp(-t/\tau), \tag{20}$$

with A a normalization factor. The spin depolarization length L is calculated by the relation $L = v_d \cdot \tau$, where v_d is the average drift velocity.

In our simulations the GaAs sample is driven by a fluctuating electric field $E(t) = E_0 + \eta(t)$, where E_0 is the amplitude of the deterministic part and $\eta(t)$ is the random contribution due to the external source of RT noise. The RT noise is generated by a random process taking only discrete values and stochastically switching between these values. We consider a symmetric dichotomous Markov stochastic process with only two values [162,163]

$$\eta(t) \in \{-\Delta, \Delta\}. \tag{21}$$

Thus, we have zero mean

$$\langle \eta(t) \rangle = 0, \tag{22}$$

and correlation function

$$\langle \eta(t)\eta(t') \rangle = \Delta^2 \exp\left(-\frac{\mid t - t' \mid}{\tau_D} \right), \tag{23}$$

where τ_D is the correlation time of the noise and it is related to the inverse of the mean frequency of transition from $\pm\Delta$ to $\mp\Delta$, respectively [162,163]. In our runs, we choose $\eta(0) = X$ as initial condition, where X is a random variable which takes the values $-\Delta$ and Δ with equal probability $(p = 1/2)$. We consider only fluctuations of equal height, in such a way that this external noise can be easily generated in practical systems and tuning effects can be more controllable.

3.3. Numerical Results and Discussion

In panels of Figure 4, we show the spin lifetime τ_0 (Figure 4a) and the spin depolarisation length L_0 (Figure 4b), respectively, as a function of the deterministic electric field amplitude E_0, at $T = 77$ K and 300 K. The spin lifetime is a monotonic decreasing function of E_0. Moreover, for field amplitudes E_0 greater than 3 kV/cm, spin lifetimes at the lattice temperature $T = 300$ K become longer than those calculated at $T = 77$ K . This unexpected finding is due to the fact that a strong value of E_0 allows that a high percentage of electrons visit the L-valleys, experiencing a spin-orbit coupling stronger than that present in the Γ-valley. This action is dominant with the respect to the disorder due to the lattice temperature. The spin relaxation length shows a nonmonotonic dependence on the electric field amplitude. The presence of a maximum at low applied electric field can be explained by the interplay between two competing factors: in the linear regime, as the field becomes larger, the electron momentum and the drift velocity increase in the direction of the field. On the other hand, the increased electron momentum also brings about a stronger effective magnetic field. For field amplitudes E_0 greater than 3 kV/cm, also the depolarization lengths L_0 calculated at the lattice temperature $T = 300$ K become greater than those obtained at nitrogenum temperature.

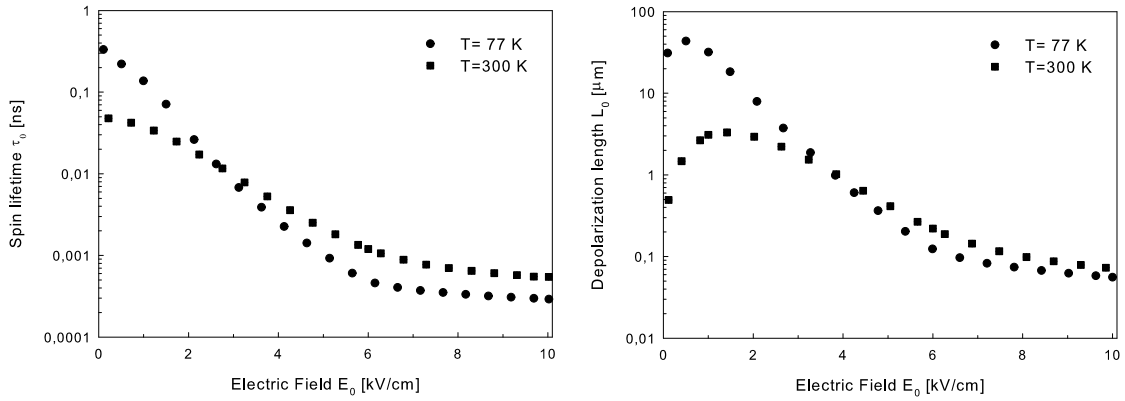

Figure 4. (**a**) Spin lifetime τ_0 and (**b**) spin relaxation length L_0 as a function of the deterministic electric field amplitude E_0, at T = 77 K and 300 K.

We here report the effects of RT external fluctuations on the spin relaxation process at room temperature ($T = 300$ K). For statistical purposes, we decided to carry out 500 different noise realisations for each strength of the deterministic applied field and evaluated both average values and error bars of the extracted spin relaxation lengths.

In panels of Figure 5, we show a single Monte Carlo realisation of the electron spin average polarisation $< S_x >$ (averaged over the electron ensemble) as a function of the distance d from the injection plane $(x_0 = 0)$. In Figure 5a the deterministic component of the fluctuating field is $E_0 = 1$ kV/cm and the RT component ha amplitude $\Delta = 0.2$ kV/cm; in Figure 5b $E_0 = 6$ kV/cm and $\Delta = 1.2$ kV/cm. τ_0 is the spin relaxation time obtained when only the deterministic field E_0 is applied. We found different results, depending on whether the deterministic field E_0 is lower or higher than the Gunn field ($F_G \approx 3.25$ kV/cm), that is the minimum value of electric field that the electrons need to move in L-valleys. In fact, in the first case the spin relaxation process is not significantly influenced by the external fluctuations for all the values of the noise characteristic time analyzed and we found a spin depolarization length almost equal to the value obtained when only the deterministic component of the driving field is applied ($L_0 = 3.1$ μm). On the other hand, if $E_0 = 6$ kV/cm, when $\tau_D \ll \tau_0$, the spin decoherence is practically not affected by the fluctuations of the electric field, which have a negligible memory (τ_D) with respect to the characteristic time τ_0 of the system, making the relaxation process quasi-deterministic.

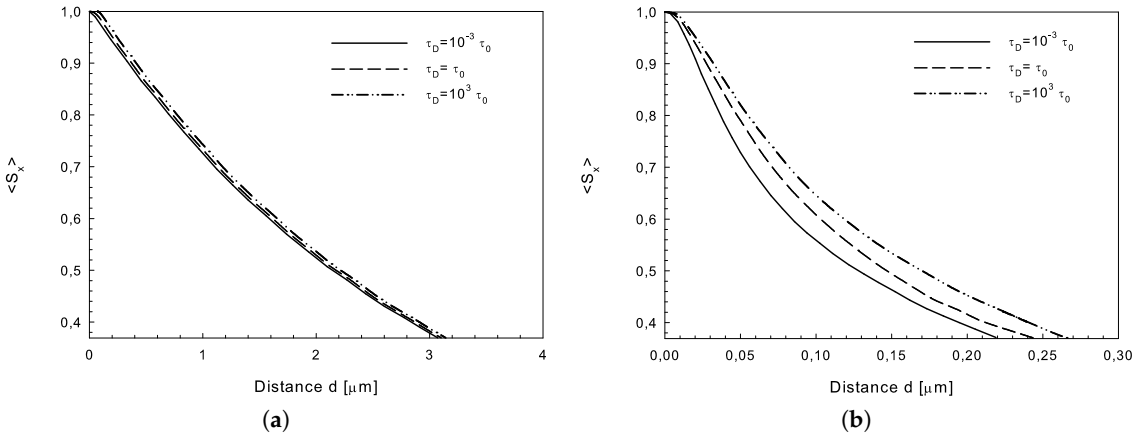

Figure 5. Spin polarisation $< S_x >$ as a function of the distance d from the injection plane ($x_0 = 0$) obtained by applying fluctuating field at three different values of the correlation τ_D, namely (solid line) $10^{-3}\tau_0$, (dashed line) τ_0 and (dashed-dotted line) $10^3\tau_0$. The other parameters are: (**a**) $E_0 = 1$ kV/cm, τ_0 =38 ps, $\Delta = 0.2$ kV/cm; (**b**) $E_0 = 6$ kV/cm, τ_0 =1.20 ps, $\Delta = 1.2$ kV/cm.

The spin dephasing process becomes to be influenced by the fluctuating field only for values of noise correlation time at least comparable with τ_0 ($\tau_D \geq \tau_0$). In these cases we found spin depolarization lengths greater than those calculated when the external fluctuations are absent (L_0=0.22 μm). In Figure 6, we show the normalised electron spin depolarization length L/L_0 as a function of the RT noise correlation time τ_D, with $E_0 = 1$ kV/cm (Figure 6a) and $E_0 = 6$ kV/cm (Figure 6b), respectively , for three different values of the RT noise amplitude Δ. When $E_0 = 1$ kV/cm, because of the amplitude of the driving field is not enough to allow the electrons to move in higher energy valleys ($E_0 < E_G$), independently on the noise mean switching time, the external fluctuations has no effect on the spin relaxation process.

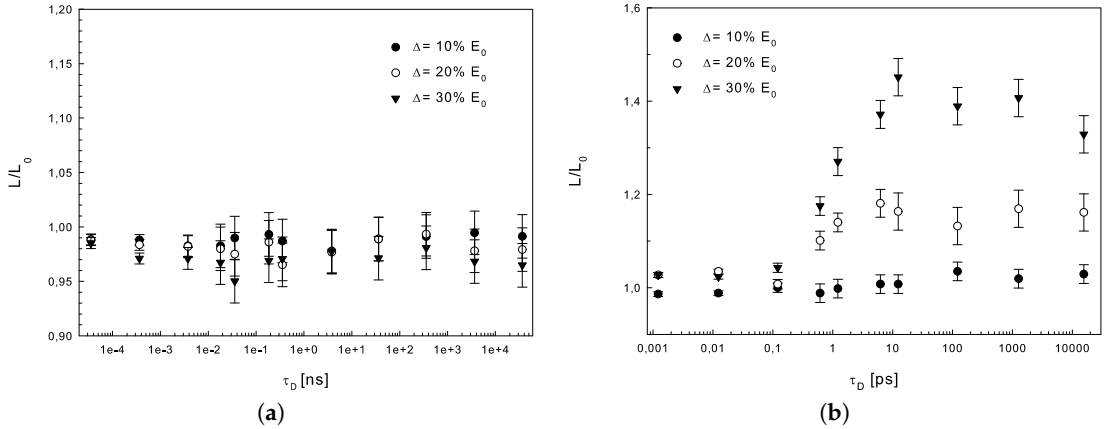

Figure 6. Normalised electron spin depolarization length L/L_0 as a function of the noise correlation time τ_D, for three different values of noise amplitude, namely Δ= 10, 20, 30 % E_0. (**a**) $E_0 = 1$ kV/cm and (**b**) $E_0 = 6$ kV/cm , respectively.

If $E_0 = 6$ kV/cm, for the lowest noise amplitude $\Delta = 0.6$ kV/cm, the electron spin depolarization length is almost constant ($L/L_0 \sim 1$), for all the values of the of the noise correlation time τ_D. When the noise amplitude increases and $\tau_D > \tau_0$, the value of the spin relaxation length Ł increase up to 1.4 L_0. For $\tau_D > 10\ \tau_0$, the electron spin relaxation length becomes constant in good approximation. This positive effect monotonically increases with the amplitude of the RT noise.

A threshold effect is observed, in which an enhancement of the electron spin relaxation length can be maintained for several orders of magnitude of the RT mean switching time, starting from

a value equal to 10 times the relaxation characteristic time of the spin system in absence of noise τ_0. The findings are very similar to those observed for the electron spin lifetimes [79] and a simple argument to explain the numerical results has been extensively discussed in [84].

4. Quantum Metastable State

The role of dissipation on the dynamics of metastable quantum system is the focus of the third system investigated. Usually, the quantum noise and/or the dissipative environment influence in a significative way the dynamics of a quantum system characterized by a metastable state. Indeed, the decay and escape rates from a metastable state have recently received increasing interest [7,86,164–168]. This problem is of general interest in many areas of physics, where the quantum systems show metastability. Here, as a model of quantum metastable system we consider a quantum particle in an asymmetric bistable potential coupled to a heat bath with Ohmic spectral density. Upon varying the strength γ of the coupling between the particle and an Ohmic environment, the escape time from a quantum metastable state exhibits a nonmonotonic behavior with a maximum. This constitutes a quantum version of the NES effect, which is a theoretically and experimentally established phenomenon [14,45,53–55], and we called it quantum noise enhanced stability (QNES) of a quantum metastable system.

In this last section the role of dissipation and temperature on the escape process of a quantum particle from a metastable state, by considering nonequilibrium initial conditions, is investigated.

4.1. The Model

The system is modeled as a particle of mass M, coordinate $\hat{q}$, and momentum $\hat{p}$, in a double–well potential V_0. The particle is linearly coupled to an environment of N independent quantum harmonic oscillators of frequencies ω_j, the so-called bosonic heat bath. The full Hamiltonian is the sum of system and bath-plus-interaction terms, according to the Caldeira-Leggett model [85,86]

$$\hat{H} = \frac{\hat{p}^2}{2M} + V_0(\hat{q}) + \sum_{j=1}^{N} \frac{1}{2}\left[\frac{\hat{p}_j^2}{m_j} + m_j\omega_j^2\left(\hat{x}_j - \frac{c_j}{m_j\omega_j^2}\hat{q}\right)^2\right]. \tag{24}$$

The constant c_j measures the coupling of the particle with the j-th oscillator. The renormalization term $\propto \hat{q}^2$ gives a spatially homogeneous dissipation, independent of $\hat{q}$. The bath spectral density function completely describes the heat bath. In the continuum limit, for Ohmic dissipation, we assume that J has the following standard form

$$J(\omega) = M\gamma\omega e^{\omega/\omega_c}, \tag{25}$$

where ω_c is a high-frequency cutoff and where the coefficient γ, which has dimension of a frequency, provides a measure of the overall coupling between the particle and the heat bath.

The static potential is parametrized by the quartic function of the particle's coordinate $\hat{x}$ [87]

$$V(\hat{x}) = \frac{M^2\omega_0^4}{64\Delta U}\hat{x}^4 - \frac{M\omega_0^2}{4}\hat{x}^2 - \epsilon\hat{x}. \tag{26}$$

Here ω_0 is the oscillation frequency around the potential minima, ϵ is a static bias and ΔU the barrier height at zero bias. In calculations we scale all the physical quantities with ω_0, which is of the same order of magnitude of the frequency spacing between ground state and the first excited energy level. We choose the parameter ϵ sufficiently large so as to attain a configuration that, in the transient dynamics, is suitable for modeling the decay in a metastable potential, starting from a nonequilibrium condition. In the upper part of Figure 7 $V(x)$ is shown for $\Delta U = 1.4\ \hbar\omega_0$ and $\epsilon = 0.27\sqrt{M\hbar\omega_0^3}$.

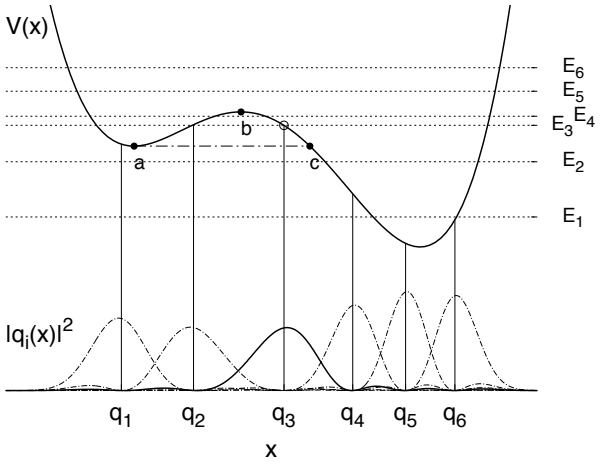

Figure 7. (Color online) Potential V (Equation (7), with $\Delta U = 1.4\hbar\omega_0$ and $\epsilon = 0.27\sqrt{M\hbar\omega_0^3}$) and first 6 energy levels (horizontal lines). In the lower part are shown the probability densities $|q_i(x)|^2 = |\langle x|q_i\rangle|^2$ associated to the DVR eigenfunctions, the initial state $|q_3\rangle$ being highlighted by a solid line. Vertical lines indicate the position eigenvalues in the DVR. The metastable region of the potential is to the left of the so-called exit point c.

4.2. Discrete Variable Representation

At low temperatures, on the energy scale set by ω_0, the time evolution of the particle is practically confined to a reduced Hilbert space spanned by the first M energy eigenstates $|E_i\rangle$, provided that the particle is not initially excited to energy levels higher than E_M. In Figure 7 the $M = 6$ case is explicitly shown for the strongly asymmetric potential used throughout the present work. In this truncated Hilbert space we perform the unitary transformation T which diagonalizes the position operator $\hat{x}$ according to

$$\begin{aligned} \mathbf{q}^{\mathrm{DVR}} &= \mathbf{T}\mathbf{x}\mathbf{T}^{\dagger} \\ &= \mathrm{diag}\{q_1, \ldots, q_M\}, \end{aligned} \tag{27}$$

where $\mathbf{x}$ is the matrix representing $\hat{x}$ in the energy basis. The resulting states

$$|q_j\rangle = \sum_{k=1}^{M} T_{jk}^{*} |E_k\rangle, \tag{28}$$

where $T_{ij} = (\mathbf{T})_{ij}$, satisfy the eigenvalue equation $\hat{x}|q_j\rangle = q_j|q_j\rangle$.

The set $\{(q_j, |q_j\rangle), \quad j = 1, \ldots, M\}$ constitutes the so-called discrete variable representation (DVR) [169,170]. The functions $q_j(x) = \langle x|q_j\rangle$ are localized around the eigenvalues q_j, as can be seen in the lower part of Figure 7: the particle in the j-th DVR state has a non-vanishing probability of being detected only in a spatial region centered around q_j. This spatially discretized picture generalizes the localized representation for a two-state system, given in terms of left/right states localized around the potential minima [86]. The DVR allows for calculating the probability of finding the particle in the region in between the minima. We exploit this possibility to study the transient dynamics in terms of escape time towards the lower well, starting from a nonequilibrium initial state (see the lower part of Figure 7). Note that spatial continuity is recovered for $M \to \infty$, i.e., removing the upper bound on the energies taken into account. The existence of intermediate localized states in the generalization of the two-state system treatment accomplished by the DVR is reflected by the multiple time scales resulting from the inclusion of energy levels above the first doublet and accounts for tunneling and intra-well relaxation [87,171].

4.3. Strong Dissipation: Analytical Approach

The populations of the DVR states $|q_j\rangle$ undergo a relaxation towards a stationary configuration which depends on the bath parameters and damping strength γ. At strong coupling this process is well approximated [171] by the incoherent relaxation captured by the master equation [172]

$$\dot{\rho}_{jj}(t) = \sum_k \Gamma_{jk}\rho_{kk}(t). \tag{29}$$

This master equation is the Markov-approximated version of the generalized master equation $\dot{\rho}_{jj}(t) = \sum_k \int_{t_0}^{t} dt' K_{jk}(t-t')\rho_{kk}(t')$ under the hypothesis that the memory time of the kernels K_{jk} is smaller than the characteristic time scale of the evolution of the populations. The time-independent rates are thus given by $\Gamma_{jk} = \int_0^\infty d\tau K_{jk}(\tau)$. The kernels K_{jk} are derived within the path integral approach to dissipation [86,173] using a multi-state generalization of the famous non-interacting blip approximation [174]. For $j \neq k$, the kernels read

$$K_{jk}(t,t') = 2\Delta_{jk}^2 e^{-q_{jk}^2 Q'(t-t')} \cos\left[\epsilon_{jk}(t-t') + q_{jk}^2 Q''(t-t')\right], \tag{30}$$

while the diagonal elements of the kernel matrix are given by $K_{kk}(t,t') = -\sum_{n\neq k} K_{nk}(t,t')$, according to the conservation of probability. In Equation (30) $\Delta_{jk} \equiv (1/\hbar)\langle q_j|\hat{H}_0|q_k\rangle$, $q_{jk} = q_j - q_k$ (q_i being the DVR eigenvalues), and $\epsilon_{jk} = \Delta_{jj} - \Delta_{kk}$. Finally, Q' and Q'' are, respectively, the real and imaginary part of the function $Q(t)$, related to the bath correlation function L by $L(t) = \hbar^2 d^2Q(t)/dt^2$. In the scaling limit set by $k_BT/\hbar\omega_c \ll 1$, we have

$$\begin{aligned} Q(t) &= Q'(t) + iQ''(t) \\ &= \frac{M\gamma}{\pi\hbar}\ln\left(\sqrt{1+\omega_c^2t^2}\frac{\sinh(\kappa t)}{\kappa t}\right) + i\frac{M\gamma}{\pi\hbar}\arctan(\omega_c t), \end{aligned} \tag{31}$$

where $\kappa = \pi k_BT/\hbar$.

The master equation (29) gives the time evolution of the populations ρ_{jj} of the DVR states. Its analytical solution reads

$$\rho_{jj}(t) = \sum_{n,k=1}^{M} S_{jn}(S^{-1})_{nk}e^{\Lambda_n(t-t_0)}\rho_{kk}(t), \tag{32}$$

where $\mathbf{S}$ is the transformation matrix diagonalizing the rate matrix $\mathbf{\Gamma}$, with eigenvalues Λ_n. The smallest, in absolute value, of the nonzero eigenvalues determines the largest time-scale of the dynamics, the quantum relaxation time τ_{relax} [87].

4.4. Escape Time

We consider the dynamics given by Equation (32) with the nonequilibrium initial condition

$$\rho(0) = |q_3\rangle\langle q_3| \tag{33}$$

i.e., with the particle initially prepared in the central region of the potential on the right of the potential barrier (see Figure 7). We choose this initial condition motivated by the investigations on the NES for classical systems, where a driven classical Brownian particle in a metastable potential is initially placed between the potential maximum and the exit point, denoted by c in Figure 7. The particle experiences an enhancement of its escape time from the metastable well for certain values of the noise intensity [14,53–55].

The escape time t_{escape} from the metastable region of the potential, the region to the left of the exit point c (see Figure 7), is defined as the time the right well population, obtained as

$$P_{\text{right}}(t) = \sum_{j=4}^{6} \rho_{jj}(t), \tag{34}$$

takes to cross a threshold value d [7] .

In the following we set the $d = 0.95$, meaning that we consider the particle escaped from the metastable region when the probability to detect it in the lower (right) well is equal or greater than 95%. Note that, due to the incoherent relaxation described by Equation (32), once the threshold is crossed no oscillatory behavior of the populations occurs. Therefore, if the population of the right well crosses the threshold at time t_{escape}, the overall population of the metastable region is not going to be larger than 0.05 at later times.

By evaluating the escape time t_{escape} from the solution (32) of the master equation for the populations the following picture emerges: As γ increases, both the escape time and the relaxation time τ_{relax} increase. This holds until a critical value of γ, dependent on the temperature, is reached. By increasing further γ the escape time steeply diminishes whereas the relaxation time continues to increase monotonically. The maxima in the escape time imply that, at a given temperature, there is an optimal value of the coupling γ for which the depletion of the metastable region is delayed. It is suggestive to address this feature as quantum noise enhanced stability (qNES) [7].

Such behavior of t_{escape} as a function of the coupling strength γ is exemplified in Figure 8 for three different temperatures T. The potential used is the one depicted in Figure 7 and the initial condition is given by Equation (33). By changing T the escape time displays the same qualitative features but the the critical coupling at which t_{escape} falls off increases with the temperature. As for the relative value of t_{escape}, it is to be noticed that, at the intermediate value of T, the escape time is lower in the whole range of γ.

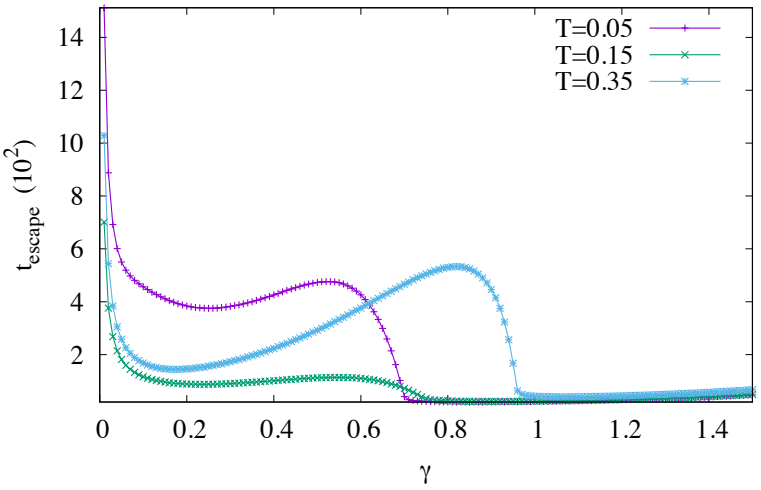

Figure 8. (Color online) Escape time (units of ω_0^{-1}) vs coupling strength γ (units of ω) for three values of the temperature (units of $\hbar\omega/k_B$). Cutoff frequency $\omega_c = 10\,\omega_0$.

To highlight this nonmonotonic behavior as a function of the temperature, in Figure 9 we plot t_{escape} as a function of the temperature for three values of the coupling strength γ: The escape time shows a minimum for all γ and, in the whole range of temperatures considered, is larger for larger γ. It should be noted that the values of the γ parameter are chosen smaller than the critical values shown in Figure 8 for a similar range of temperatures.

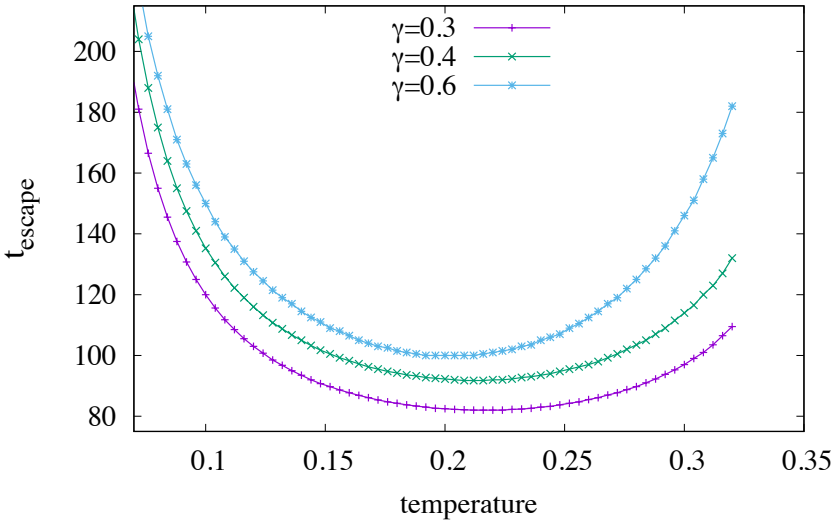

Figure 9. (Color online) Escape time (units of ω_0^{-1}) vs temperature (units of $\hbar\omega/k_B$) for three values of the coupling γ (units of ω_0). Cutoff frequency $\omega_c = 10\,\omega_0$.

5. Conclusions

Three nonlinear relaxation phenomena induced by the noise in condensed matter systems have been investigated. In particular, the noise enhanced stability (NES), the stochastic resonant activation (SRA) and the noise-induced coherence of electron spin (NCS) have been analyzed in Josephson junctions, n-doped GaAs semiconductor crystal, and quantum metastable system.

(i) The transient dynamics of short and long JJs, in the presence of Gaussian and non-Gaussian noise sources, has been analyzed.

Specifically, the short JJ has a graphene sheet as an interlayer and this gives rise to a nonsinusoidal behavior of the Josephson current. The underdamped SGS JJ has been subject to an external periodical driving current and a stochastic Gaussian noise current. Two noise induced phenomena, namely the NES and SRA, have been observed, and the role of a randomly distributed phase of the driving periodical signal in the dynamics of a SGS JJ has been investigated. We find that one of the two minima of the dynamical resonant activation phenomenon disappears with a random initial phase, while the NES effect persists. To analyze in more detail the NES phenomenon in both cases of zero phase or randomly distributed phase, the probability density functions of the switching times have been calculated.

The dynamics of a long JJ has been investigated in the presence of a non-Gaussian dichotomous noise with different initial conditions for the noise source (up, down and random). The effects of these different initial conditions on the noise induced effects (NES and SRA) have been investigated. In particular, the SRA is always observed by varying the initial condition of the non-Gaussian noise. However, for certain initial conditions of the dichotomous noise, that is β_{up}, the NES effect disappears. For this choice of values of system and noise parameters, the escape process is speeded up and the peculiar trapping phenomenon of the NES effect is not observed. For the other two initial values of $\beta(t)$, namely down and random, the NES phenomenon is observed (see Figure 3e,f).

(ii) We have analyzed the influence of RT external fluctuations on the electron spin relaxation process in n-doped GaAs semiconductor bulks. Our numerical results show that if the deterministic component of the driving electric field has amplitude greater than the Gunn threshold, it is possible to enhance the depolarization length up to 40% of its value in the absence of external noise. This effect increases with the amplitude of the external fluctuations, but it is observed only for noise correlation times comparable to or greater than the spin lifetime obtained with the only deterministic applied field (threshold effect). This positive effect, obtainable in a wide range of noise correlation times, is

ascribed to the different effective electric field experienced by the electron ensemble, within the time window of the spin relaxation time, is associated to a decrease of the occupation of the *L*-valleys, where the strength of spin-orbit coupling felt by electrons is at least one order of magnitude greater than that present in Γ-valley.

Our findings show that, by superimposing this fluctuations source to the intrinsic one, it is possible to adjust the speed of the spin relaxation dynamics of the system. In particular, for electric field strengths greater than the Gunn's field, the depolarization length is enhanced by increasing both the amplitude and the characteristic time of the external noise, while in low-field conditions, the spin relaxation process is not influenced by the external fluctuations.

External random fluctuations suitably superimposed to the electric driving field, could play a very important role on controlling and tuning the spin relaxation processes. In fact, on the wake of our findings, by using appropriate noise characteristic times and amplitudes, could be possible to select the most favorable condition for using the electron spin to carry the information.

(iii) We have investigated the transient dynamics of a quantum metastable system in the presence of strong Ohmic dissipation. This was done by considering the escape time from the metastable region, the region to the left of the exit point of the potential (point *c* in Figure 7), starting from a nonequilibrium initial condition. The initial condition considered is substantially different from the quasi-equilibrium state inside the metastable well used in quantum rates calculations [88,89]. The preparation is indeed assumed to be of the kind used for classical system where NES is predicted, namely the particle initially in a nonequilibrium position between the top of the barrier and the so-called exit point of the potential see Figure 7.

Nonmonotonic behavior of the escape time as a function both of coupling strength and temperature has been observed in the quantum metastable system. A maximization of the escape time was found at specific, temperature-dependent, values of the coupling strength, in close analogy with the noise enhanced stability in metastable classical systems. We call this the quantum noise enhanced stability phenomenon: strong dissipation due to the system-bath coupling enhances the stability of the metastable system in the quantum regime.

Acknowledgments: This work was partly supported by MIUR and CNISM. Claudio Guarcello has received funding from the European Union FP7/2007-2013 under REA grant agreement no 630925 – COHEAT and from MIUR-FIRB2013 – Project Coca (Grant No. RBFR1379UX).

Author Contributions: Bernardo Spagnolo and Davide Valenti conceived, obtained and interpreted the results, and made the preparation of all entire paper. Claudio Guarcello contributed to conceived, obtained and interpreted the results of the section 2 of the paper. Dominique Persano Adorno contributed to conceived, obtained and interpreted the results of the section 3 of the paper. Luca Magazzù and Angelo Carollo contributed to conceived, obtained and interpreted the results of the section 4 of the paper. All authors have read and approved the final manuscript.

Conflicts of Interest: The authors declare no conflict of interest.

References

1. Bars, I.; Steinhardt, P.J.; Turok, N. Cyclic cosmology, conformal symmetry and the metastability of the Higgs. *Phys. Lett. B* **2013**, *726*, 50–55.
2. Espinosa, J.R.; Giudice, G.F.; Riotto A. Cosmological implications of the Higgs mass measurement. *J. Cosmol. Astropart. Phys.* **2008**, *2008*, doi:10.1088/1475-7516/2008/05/002.
3. Steinhardt, P.J.; Turok, N. A Cyclic Model of the Universe. *Science* **2002**, *296*, 1436–1439.
4. Steinhardt, P.J.; Turok, N. Cosmic evolution in a cyclic universe. *Phys. Rev. D* **2002**, *65*, 126003.
5. Bovier, A.; den Hollander, F. *Metastability. A Potential-Theoretic Approach*; Springer: Berlin/Heidelberg, Germany, 2015.
6. Serdukova, L.; Zheng, Y.; Duan, J.; Kurths, J. Stochastic basins of attraction for metastable states. *Chaos* **2016**, *26*, 073117.
7. Valenti, D.; Magazzù, L.; Caldara, P.; Spagnolo, B. Stabilization of quantum metastable states by dissipation. *Phys. Rev. B* **2015**, *91*, 235412.

8. Menck, P.; Heitzing, J.; Marwan, N.; Kurths, J. How basin stability complements the linear-stability paradigm. *Nat. Phys.* **2013**, *9*, 89–92.
9. Oliveiri, E.; Vares, M. *Large Deviations and Metastability*; Cambridge University Press: Cambridge, UK, 2004.
10. Scütte, C.; Sarich, M. *Metastability and Markov State Models in Molecular Dynamics*; American Mathematical Society: Providence, RI, USA, 2013.
11. Beltrán, J.; Landim, C. Tunneling and metastability of continuous time Markov chains II, the nonreversible case. *J. Stat. Phys.* **2012**, *149*, 598–618.
12. Giardina, I. Metastable states in glassy systems. In *Les Houches—Session LXXXV: Complex Systems*; Bouchaud, J.-P., Mezard, M., Dalibard, J., Eds.; Elsevier: Amsterdam, The Netherlands, 2007; pp. 373–394.
13. Bouchaud, J.-P.; Mezard, M.; Dalibard, J. (Eds.) *Les Houches—Session LXXXV: Complex Systems*; Elsevier: Amsterdam, The Netherlands, 2007.
14. Dubkov, A.A.; Agudov, N.V.; Spagnolo, B. Noise-enhanced stability in fluctuating metastable states. *Phys. Rev. E* **2004**, *69*, 061103.
15. Spagnolo, B.; Dubkov, A.A.; Agudov, N.V. Enhancement of stability in randomly switching potential with metastable state. *Eur. Phys. J. B* **2004**, *40*, 273–281.
16. Augello, G.; Valenti, D.; Spagnolo, B. Non-Gaussian noise effects in the dynamics of a short overdamped Josephson junction. *Eur. Phys. J. B* **2010**, *78*, 225–234.
17. Valenti, D.; Guarcello, C.; Spagnolo, B. Switching times in long-overlap Josephson junctions subject to thermal fluctuations and non-Gaussian noise sources. *Phys. Rev. B* **2014**, *89*, 214510.
18. Vilar, J.M.G.; Rubi, J.M. Noise Suppression by Noise. *Phys. Rev. Lett.* **2001**, *86*, 950–953.
19. Ciuchi, S.; de Pasquale, F.; Spagnolo, B. Nonlinear Relaxation in the presence of an Absorbing Barrier. *Phys. Rev. E* **1993**, *47*, 3915–3926.
20. Seol, Y.; Visscher, K.; Walton, D.B. Suppression of Noise in a Noisy Optical Trap. *Phys. Rev. Lett.* **2004**, *93*, 160602.
21. Walton, D.B.; Visscher, K. Noise suppression and spectral decomposition for state-dependent noise in the presence of a stationary fluctuating input. *Phys. Rev. E* **2004**, *69*, 051110.
22. Valenti, D.; Augello, G.; Spagnolo, B. Dynamics of a FitzHugh-Nagumo system subjected to autocorrelated noise. *Eur. Phys. J. B* **2008**, *65*, 443–451.
23. Fiasconaro, A.; Spagnolo, B. Stability measures in metastable states with Gaussian colored noise. *Phys. Rev. E* **2009**, *80*, 041110.
24. Romanczuk, P.; Bär, M.; Ebeling, W.; Lindner, B.; Schimansky-Geier, L. Active Brownian particles. *Eur. Phys. J. Spec. Top.* **2012**, *202*, 1–162, doi:10.1140/epjst/e2012-01529-y.
25. Sonnenschein, B.; Schimansky-Geier, L. Onset of synchronization in complex networks of noisy oscillators. *Phys. Rev. E* **2012**, *85*, 051116.
26. Martens, S.; Straube, A.V.; Schmid, G.; Schimansky-Geier, L.; Hänggi, P. Hydrodynamically Enforced Entropic Trapping of Brownian Particles. *Phys. Rev. Lett.* **2013**, *110*, 010601.
27. Kromer, J.A.; Pinto, R.D.; Lindner, B.; Schimansky-Geier, L. Noise-controlled bistability in an excitable system with positive feedback. *Europhys. Lett.* **2014**, *108*, 20007.
28. Sonnenschein, B.; Peron, T.K.D.M.; Rodrigues, F.A.; Kurths, J.; Schimansky-Geier, L. Cooperative behavior between oscillatory and excitable units: The peculiar role of positive coupling-frequency correlations. *Eur. Phys. J. B* **2014**, *87*, 182.
29. Dugaev, V.K.; Inglot, M.; Sherman, E.Y.; Barnas, J. Spin Hall effect and spin current generation in two-dimensional systems with random Rashba spin-orbit coupling. *J. Magn. Magn. Mater.* **2012**, *324*, 3573–3575.
30. Ghosh, P.; Chattopadhyay, S.; Chaudhuri, J.R. Enhancement of current commensurate with mutual noise-noise correlation in a symmetric periodic substrate: The benefits of noise and nonlinearity. *Chem. Phys.* **2012**, *402*, 48–55.
31. Sen, M.K.; Ray, S.; Baura, A.; Bag, B.C. Effect of multiplicative noise on the self-induced aggregation kinetics of Brownian particles. *Chem. Phys. Lett.* **2013**, *559*, 117–122.
32. Yoshimoto, M.; Shirahama, H.; Kurosawa, S. Noise-induced order in the chaos of the Belousov–Zhabotinsky reaction. *J. Chem. Phys.* **2008**, *129*, 014508.
33. Pizzolato, N.; Fiasconaro, A.; Adorno, D.P.; Spagnolo, B. Resonant activation in polymer translocation: New insights into escape dynamics of molecules driven by an oscillating field. *Phys. Biol.* **2010**, *7*, 034001.

34. Valenti, D.; Denaro, G.; Adorno, D.P.; Pizzolato, N.; Zammito, S.; Spagnolo, B. Monte Carlo analysis of polymer translocation with deterministic and noisy electric fields. *Cent. Eur. J. Phys.* **2012**, *10*, 560–567.
35. Pizzolato, N.; Fiasconaro, A.; Adorno, D.P.; Spagnolo, B. Translocation dynamics of a short polymer driven by an oscillating force. *J. Chem. Phys.* **2013**, *138*, 054902.
36. Atxitia, U.; Chubykalo-Fesenko, O.; Chantrell, R.W.; Nowak, U.; Rebei A. Ultrafast Spin Dynamics: The Effect of Colored Noise. *Phys. Rev. Lett.* **2009**, *102*, 057203.
37. Trapanese, M. Noise enhanced stability in magnetic systems. *J. Appl. Phys.* **2009**, *105*, doi:10.1063/1.3075864.
38. Adorno, D.P.; Capizzo, M.C.; Zarcone, M. Changes of electronic noise induced by oscillating fields in bulk GaAs semiconductors. *Fluct. Noise Lett.* **2008**, *8*, L11–L22.
39. Adorno, D.P.; Pizzolato, N.; Spagnolo, B. External Noise Effects on the Electron Velocity Fluctuations in Semiconductors. *Acta Phys. Pol. A* **2008**, *113*, 985–988.
40. Adorno, D.P.; Pizzolato, N.; Spagnolo, B. Noise influence on electron dynamics in semiconductors driven by a periodic electric field. *J. Stat. Mech. Theory Exp.* **2009**, doi:10.1088/1742-5468/2009/01/P01039.
41. Adorno, D.P.; Pizzolato, N.; Valenti, D.; Spagnolo, B. External noise effects in doped semiconductors operating under sub-THz signals. *Rep. Math. Phys.* **2012**, *70*, 171–179.
42. Adorno, D.P.; Pizzolato, N.; Alaimo, P.; Spagnolo, B.; Di Paola, B. Electron dynamical response in InP semiconductors driven by fluctuating electric fields. *Chaos Soliton Fract.* **2015**, *81*, 425–431.
43. Adorno, D.P.; Pizzolato, N.; Spagnolo, B. Noise-induced resonance-like phenomena in InP crystals embedded in fluctuating electric fields. *J. Stat. Mech. Theory Exp.* **2016**, *2016*, 054021.
44. Lodato, M.A.; Adorno, D.P.; Pizzolato, N.; Spezia, S.; Spagnolo, B. External Noise Effects in Silicon MOS Inversion Layer. *Acta Phys. Pol. B* **2013**, *44*, 1163–1172.
45. Spagnolo, B.; Dubkov, A.; Pankratov, A.; Pankratova, E.; Fiasconaro, A.; Ochab-Marcinek, A. Lifetime of metastable states and suppression of noise in interdisciplinary physical models. *Acta Phys. Pol. B* **2007**, *38*, 1925–1950.
46. Bonanno, G.; Valenti, D.; Spagnolo, B. Mean escape time in a system with stochastic volatility. *Phys. Rev. E* **2007**, *75*, 016106.
47. Mankin, R.; Soika, E.; Sauga, A.; Ainsaar, A. Thermally enhanced stability in fluctuating bistable potentials. *Phys. Rev. E* **2008**, *77*, 051113.
48. Valenti, D.; Spagnolo, B.; Bonanno, G. Hitting time distributions in financial markets. *Physica A* **2007**, *382*, 311–320.
49. Mantegna, R.N.; Spagnolo, B. Probability distribution of the Residence Times in Periodically Fluctuating Metastable Systems. *Int. J. Bifurc. Chaos* **1998**, *8*, 783–790.
50. Bonanno, G.; Valenti, D.; Spagnolo, B. Role of Noise in a Market Model with Stochastic Volatility. *Eur. Phys. J. B* **2006**, *53*, 405–409.
51. Agudov, N.V.; Dubkov, A.A.; Spagnolo, B. Escape from a metastable state with fluctuating barrier. *Physica A* **2003**, *325*, 144–151.
52. Spagnolo, B.; Agudov, N.V.; Dubkov, A.A. Noise enhanced stability. *Acta Phys. Pol. B* **2004**, *35*, 1419–1436.
53. Mantegna, R.; Spagnolo, B. Noise Enhanced Stability in an Unstable System. *Phys. Rev. Lett.* **1996**, *76*, 563–566.
54. Agudov, N.V.; Spagnolo, B. Noise-enhanced stability of periodically driven metastable states. *Phys. Rev. E* **2001**, *64*, 035102.
55. Fiasconaro, A.; Spagnolo, B.; Boccaletti, S. Signatures of noise-enhanced stability in metastable states. *Phys. Rev. E* **2005**, *72*, 061110.
56. Fiasconaro, A.; Mazo, J.J.; Spagnolo, B. Noise-induced enhancement of stability in a metastable system with damping. *Phys. Rev. E* **2010**, *82*, 041120.
57. Agudov, N.V.; Malakhov, A.N. Decay of unstable equilibrium and nonequilibrium states with inverse probability current taken into account. *Phys. Rev. E* **1999**, *60*, 6333–6342.
58. Dan, D.; Mahato, M.C.; Jayannavar, A.M. Mobility and stochastic resonance in spatially inhomogeneous systems. *Phys. Rev. E* **1999**, *60*, 6421–6428.
59. Wackerbauer, R. When noise decreases deterministic diffusion. *Phys. Rev. E* **1999**, *59*, 2872–2879.
60. Mielke, A. Noise Induced Stability in Fluctuating, Bistable Potentials. *Phys. Rev. Lett.* **2000**, *84*, 818–821.

61. Pankratov, A.L.; Spagnolo, B. Suppression of timing errors in short overdamped Josephson junctions. *Phys. Rev. Lett.* **2004**, *93*, 177001.
62. D'Odorico, P.; Laio, F.; Ridolfi, L. Noise-induced stability in dryland plant ecosystems. *Proc. Natl. Acad. Sci. USA* **2005**, *102*, 10819–10822.
63. Hurtado, P.I.; Marro, J.; Garrido, P. Metastability, nucleation, and noise-enhanced stabilization out of equilibrium. *Phys. Rev. E* **2006**, *74*, 050101.
64. Li, J.H.; Łuczka, J. Thermal-inertial ratchet effects: Negative mobility, resonant activation, noise-enhanced stability, and noise-weakened stability. *Phys. Rev. E* **2010**, *82*, 041104.
65. Smirnov, A.A.; Pankratov, A.L. Influence of the size of uniaxial magnetic nanoparticle on the reliability of high-speed switching. *Phys. Rev. B* **2010**, *82*, 132405.
66. Jia, Z.-L.; Mei, D.-C. Effects of linear and nonlinear time-delayed feedback on the noise-enhanced stability phenomenon in a periodically driven bistable system. *J. Stat. Mech. Theory Exp.* **2011**, *2011*, doi:10.1088/1742-5468/2011/10/P10010.
67. Parker, M.; Kamenev, A.; Meerson, B. Noise-induced stabilization in population dynamics. *Phys. Rev. Lett.* **2011**, *107*, 180603.
68. Kramers, H.A. Brownian Motion in a Field of Force and the Diffusion Model of Chemical Reactions. *Physica* **1940**, *7*, 284–304.
69. Hänggi, P.H.; Talkner, P.; Borkovec, M. Reaction Rate Theory: Fifty Years After Kramers. *Rev. Mod. Phys.* **1990**, *62*, 251–342.
70. Reimann, P.; Van den Broeck, C.; Linke, H.; Hänggi, P.; Rubi, J.; Pérez-Madrid, A. Giant acceleration of free diffusion by use of tilted periodic potentials. *Phys. Rev. Lett.* **2001**, *87*, 010602.
71. Dubkov, A.A.; Spagnolo, B. Acceleration of diffusion in randomly switching potential with supersymmetry. *Phys. Rev. E* **2005**, *72*, 041104.
72. Wendin, G.; Shumeiko, V.S. Quantum bits with Josephson junctions. *Low Temp. Phys.* **2007**, *33*, 724–744.
73. Kim, J.H.; Dhungana, R.P.; Park, K.-S. Decoherence in Josephson vortex quantum bits: Long-Josephson-junction approach to a two-state system. *Phys. Rev. B* **2006**, *73*, 214506.
74. Szombati, D.B.; Nadj-Perge, S.; Car, D.; Plissard, S.R.; Bakkers, E.P.A.M.; Kouwenhoven, L.P. Josephson Φ_0-junction in nanowire quantum dots. *Nat. Phys.* **2016**, *12*, 568–572.
75. Levenson-Falk, E.M.; Vijay, R.; Antler, N.; Siddiqi, I. A dispersive nanoSQUID magnetometer for ultra-low noise, high bandwidth flux detection. *Supercond. Sci. Technol.* **2013**, *26*, 055015.
76. Grabert, H. Theory of a Josephson junction detector of non-Gaussian noise. *Phys. Rev. B* **2008**, *77*, 205315 .
77. Filatrella, G.; Pierro, V. Detection of noise-corrupted sinusoidal signals with Josephson junctions. *Phys. Rev. E* **2010**, *82*, 046712.
78. Addesso, P.; Filatrella, G.; Pierro, V. Characterisation of escape times of Josephson junctions for signal detection. *Phys. Rev. E* **2012**, *85*, 016708.
79. Spagnolo, B.; Valenti, D.; Guarcello, C.; Carolllo, A.; Adorno, D.P.; Spezia, S.; Pizzolato, N; Di Paola, B. Noise-induced effects in nonlinear relaxation of condensed matter systems. *Chaos Soliton Fract.* **2015**, *81*, 412–424.
80. Guarcello, C.; Valenti, D.; Spagnolo, B. Phase dynamics in graphene-based Josephson junctions in the presence of thermal and correlated fluctuations. *Phys. Rev. B* **2015**, *92*, 174519.
81. Guarcello, C.; Valenti, D.; Carollo, A.; Spagnolo, B. Effects of Lévy noise on the dynamics of sine-Gordon solitons in long Josephson junctions. *J. Stat. Mech. Theory Exp.* **2016**, *2016*, doi:10.1088/1742-5468/2016/05/054012.
82. Spezia, S.; Adorno, D.P.; Pizzolato, N.; Spagnolo, B. New insights into electron spin dynamics in the presence of correlated noise. *J. Phys. Condens. Matter* **2012**, *24*, 052204.
83. Spezia, S.; Adorno, D.P.; Pizzolato, N.; Spagnolo, B. Effect of a Fluctuating Electric Field on Electron Spin Dephasing Time in III-V Semiconductors. *Acta Phys. Pol. B* **2012**, *43*, 1191–1201.
84. Spezia, S.; Adorno, D.P.; Pizzolato, N.; Spagnolo, B. Enhancement of electron spin lifetime in GaAs crystals: The benefits of dichotomous noise. *Eur. Phys. Lett.* **2013**, *104*, 47011.
85. Caldeira, A.O.; Leggett, A.J. Influence of Dissipation on Quantum Tunneling in Macroscopic Systems. *Phys. Rev. Lett.* **1981**, *46*, 211–214.
86. Weiss, U. *Quantum Dissipative Systems*, 4th ed.; World Scientific: Singapore, Singapore, 2012.

87. Thorwart, M.; Grifoni, M.; Hänggi, P. Strong Coupling Theory for Tunneling and Vibrational Relaxation in Driven Bistable Systems. *Ann. Phys.* **2001**, *293*, 15–66.
88. Affleck, I. Quantum-Statistical Metastability. *Phys. Rev. Lett.* **1981**, *46*, 388–391.
89. Grabert, H.; Olschowski, P.; Weiss, U. Quantum decay rates for dissipative systems at finite temperatures. *Phys. Rev. B* **1987**, *36*, 1931–1951.
90. Barone, A.; Paterno, G. *Physics and Applications of the Josephson Effect*; Wiley: New York, NY, USA, 1982.
91. Guarcello, C.; Valenti, D.; Carollo, A.; Spagnolo, B. Stabilization Effects of Dichotomous Noise on the Lifetime of the Superconducting State in a Long Josephson Junction. *Entropy* **2015**, *17*, 2862–2875.
92. Novotný T. Josephson junctions as threshold detectors of full counting statistics: Open issues. *J. Stat. Mech. Theory Exp.* **2009**, doi:10.1088/1742-5468/2009/01/P01050.
93. Tobiska, J.; Nazarov, Y.V. Josephson junctions as threshold detectors for full counting statistics. *Phys. Rev. Lett.* **2004**, *93*, 106801.
94. Sukhorukov, E.V.; Jordan, A.N. Stochastic dynamics of a Josephson junction threshold detector. *Phys. Rev. Lett.* **2007**, *98*, 136803.
95. Dubkov, A.A.; Spagnolo, B. Langevin Approach to Lévy flights in fixed potentials: Exact results for stationary probability distributions. *Acta Phys. Pol. B* **2007**, *38*, 1745–1758.
96. Ankerhold, J. Detecting charge noise with a Josephson junction: A problem of thermal escape in presence of non-Gaussian fluctuations. *Phys. Rev. Lett.* **2007**, *98*, 036601.
97. Lee, G.-H.; Jeong, D.; Choi, J.-H.; Doh, Y.-J.; Lee, H.-J. Electrically tunable macroscopic quantum tunnelling in a graphene-based Josephson junction. *Phys. Rev. Lett.* **2011**, *107*, 146605.
98. Choi, J.-H.; Lee, G.-H.; Park, S.; Jeong, D.; Lee, J.-O.; Sim, H.-S.; Doh, Y.-J.; Lee, H.-J. Complete gate control of supercurrent in graphene p–n junctions. *Nat. Commun.* **2013**, *4*, 2525.
99. Heersche, H.B.; Jarillo-Herrero, P.; Oostinga, J.B.; Vandersypen, L.M.; Morpurgo, A.F. Bipolar supercurrent in graphene *Nature* **2007**, *446*, 56–59.
100. Du, X.; Skachko, I.; Andrei, E.Y. Josephson current and multiple Andreev reflections in graphene sns junctions. *Phys. Rev. B* **2008**, *77*, 184507.
101. Miao, F.; Wijeratne, S.; Zhang, Y.; Coskun, U.C.; Bao, W.; Lau, C.N. Phase-coherent transport in graphene quantum billiards. *Science* **2007**, *317*, 1530–1533.
102. Jeong, D.; Choi, J.-H.; Lee, G.-H.; Jo, S.; Doh, Y.-J.; Lee, H.-J. Observation of supercurrent in PbIn-graphene-PbIn Josephson junction. *Phys. Rev. B* **2011**, *83*, 094503.
103. Coskun, U.; Brenner, M.; Hymel, T.; Vakaryuk, V.; Levchenko, A.; Bezryadin, A. Distribution of supercurrent switching in graphene under the proximity effect. *Phys. Rev. Lett.* **2012**, *108*, 097003.
104. Mizuno, N.; Nielsen, B.; Du, X. Ballistic-like supercurrent in suspended graphene Josephson weak links. *Nat. Commun.* **2013**, *4*, 2716.
105. Kogan, S. *Electronic Noise and Fluctuations in Solids*; Cambridge University Press: Cambridge, UK, 1996.
106. Pankratov, E.; Spagnolo, B. Optimization of impurity profile for p-n-junction in heterostructures. *Eur. Phys. J. B* **2005**, *46*, 15–19.
107. Ustinov, A. Solitons in Josephson junctions. *Physica D* **1998**, *123*, 315–329.
108. Büttiker, M.; Landauer, R. Nucleation theory of overdamped soliton motion. *Phys. Rev. A* **1981**, *23*, 1397–1410.
109. McLaughlin, D.W.; Scott, A.C. Perturbation analysis of fluxon dynamics. *Phys. Rev. A* **1978**, *18*, 1652–1680.
110. Dueholm, B.; Joergensen, E.; Levring, O.; Monaco, R.; Mygind, J.; Pedersen, N.; Samuelsen, M. An analysis of fluxons in long Josephson junctions. *IEEE Trans. Magn.* **1983**, *19*, 1196–1200.
111. Titov, M.; Beenakker, C.W. Josephson effect in ballistic graphene. *Phys. Rev. B* **2006**, *74*, 041401.
112. Hagymási, I.; Kormányos, A.; Cserti, J. Josephson current in ballistic superconductor-graphene systems. *Phys. Rev. B* **2010**, *82*, 134516.
113. Devoret, M.H.; Martinis, J.M.; Esteve, D.; Clarke, J. Resonant activation from the zero-voltage state of a current-biased Josephson junction. *Phys. Rev. Lett.* **1984**, *53*, 1260–1263.
114. Devoret, M.H.; Martinis, J.M.; Clarke, J. Measurements of macroscopic quantum tunneling out of the zero-voltage state of a current-biased Josephson junction. *Phys. Rev. Lett.* **1985**, *55*, 1908–1911.
115. Martinis, J.M.; Devoret, M.H.; Clarke, J. Experimental tests for the quantum behavior of a macroscopic degree of freedom: The phase difference across a Josephson junction. *Phys. Rev. B* **1987**, *35*, 4682–4698.

116. Fiasconaro, A.; Spagnolo, B. Resonant activation in piecewise linear asymmetric potentials. *Phys. Rev. E* **2011**, *83*, 041122.
117. Pan, C.; Tan, X.; Yu, Y.; Sun, G.; Kang, L.; Xu, W.; Chen, J.; Wu, P. Resonant activation through effective temperature oscillation in a Josephson tunnel junction. *Phys. Rev. E* **2009**, *79*, 030104.
118. Mantegna, R.; Spagnolo, B. Numerical simulation of resonant activation in a fluctuating metastable model system. *J. Phys. IV (France)* **1998**, *8*, 247–251.
119. Fedorov, K.; Pankratov, A.L.; Spagnolo, B. Influence of length on the noise delayed switching of long Josephson junctions. *Int. J. Bifurc. Chaos* **2008**, *18*, 2857–2862.
120. Fedorov, K.; Pankratov, A. Mean time of the thermal escape in a current-biased long-overlap Josephson junction. *Phys. Rev. B* **2007**, *76*, 024504.
121. Augello, G.; Valenti, D.; Pankratov, A.L.; Spagnolo, B. Lifetime of the superconductive state in short and long Josephson junctions. *Eur. Phys. J. B* **2009**, *70*, 145–151.
122. Pankratov, A.L.; Gordeeva, A.V.; Kuzmin, L.S. Drastic Suppression of Noise-Induced Errors in Underdamped Long Josephson Junctions. *Phys. Rev. Lett.* **2012**, *109*, 087003.
123. Guarcello, C.; Valenti, D.; Augello, G.; Spagnolo, B. The Role of Non-Gaussian Sources in the Transient Dynamics of Long Josephson Junctions. *Acta Phys. Pol. B* **2013**, *44*, 997–1005.
124. Valenti, D.; Schimansky-Geier, L.; Sailer, X.; Spagnolo, B. Moment equations for a spatially extended system of two competing species. *Eur. Phys. J. B* **2006**, *50*, 199–203.
125. Valenti, D.; Schimansky-Geier, L.; Sailer, X.; Spagnolo, B.; Iacomi, M. Moment Equations in a Lotka–Volterra Extended System with Time Correlated Noise. *Acta Phys. Pol. B* **2007**, *38*, 1961–1972.
126. Valenti, D.; Spagnolo, B. Stochastic dynamics and mean field approach in a system of three interacting species. *Cent. Eur. J. Phys.* **2009**, *7*, 457–471.
127. Valenti, D.; Pizzolato, N.; Spagnolo, B. Mean Field Approach and Role of the Coloured Noise in the Dynamics of Three Interacting Species. *Acta Phys. Pol. B* **2010**, *41*, 1051–1071.
128. Doering, C.R.; Gadoua, J.C. Resonant activation over a fluctuating barrier. *Phys. Rev. Lett.* **1992**, *69*, 2318–2321.
129. Mantegna, R.N.; Spagnolo, B. Experimental investigation of resonant activation. *Phys. Rev. Lett.* **2000**, *84*, 3025–3028.
130. Pechukas, P.; Hänggi, P. Rates of activated processes with fluctuating barriers. *Phys. Rev. Lett.* **1994**, *73*, 2772–2775.
131. Marchi, M.; Marchesoni, F.; Gammaitoni, L.; Menichella-Saetta, E.; Santucci, S. Resonant activation in a bistable system. *Phys. Rev. E* **1996**, *54*, 3479–3487.
132. Fiasconaro A.; Ochab–Marcinek A.; Spagnolo B.; Gudowska–Nowak E. Monitoring noise-resonant effects in cancer growth influenced by spontaneous fluctuations and periodic treatment. *Eur. Phys. J. B* **2008**, *65*, 435–442.
133. Dybiec, B.; Gudowska-Nowak, E. Lévy stable noise-induced transitions: Stochastic resonance, resonant activation and dynamic hysteresis. *J. Stat. Mech. Theory Exp.* **2009**, doi:10.1088/1742-5468/2009/05/P05004.
134. Miyamoto, S.; Nishiguchi, K.; Ono, Y.; Itoh, K.M.; Fujiwara, A. Resonant escape over an oscillating barrier in a single-electron ratchet transfer. *Phys. Rev. B* **2010**, *82*, 033303.
135. Hasegawa, Y.; Arita, M. Escape process and stochastic resonance under noise intensity fluctuation. *Phys. Lett. A* **2011**, *375*, 3450–3458.
136. Wolf, S.A.; Awschalom, D.D.; Buhrman, R.A.; Daughton, J.M.; Von Molnár, S.; Roukes, M.L.; Chtchelkanova, A.Y.; Treger, D.M. Spintronics: A Spin-Based Electronics Vision for the Future. *Science* **2001**, *294*, 1488–1495.
137. Žutić, I.; Fabian, J.; Das Sarma, S. Spintronics: Fundamentals and applications. *Rev. Mod. Phys.* **2004**, *76*, 323–410.
138. Fabian, J.; Matos-Abiague, A.; Ertler, C.; Stano, P.; Žutić, I. Semiconductor Spintronics. *Acta Phys. Slovaca* **2007**, *57*, 565–907.
139. Behin-Aein, B.; Datta, D.; Salahuddin, S.; Datta, S. Proposal for an all-spin logic device with built-in memory. *Nat. Nanotechnol.* **2010**, *5*, 266–270.
140. Pulizzi, F. Spintronics. *Nat. Mater.* **2012**, *11*, doi:10.1038/nmat3327.
141. Salahuddin, S. Solid-state physics: A new spin on spintronics. *Nature* **2013**, *494*, 43–44.

142. Cadiz, F.; Barate, P.; Paget, D.; Grebenkov, D.; Korb, J. P.; Rowe, A.C.H.; Amand, T.; Arscott, S.; Peytavit, E. All optical method for investigation of spin and charge transport in semiconductors: Combination of spatially and time-resolved luminescence. *J. Appl. Phys.* **2014**, *116*, 023711.
143. Datta, S.; Das, B. Electronic analog of the electro-optic modulator. *Appl. Phys. Lett.* **1990**, *56*, 665–667.
144. Awschalom, D.D.; Bassett, L.C.; Dzurak, A.S.; Hu, E.L.; Petta, J.R. Quantum Spintronics: Engineering and Manipulating Atom-Like Spins in Semiconductors. *Science* **2013**, *339*, 1174–1179.
145. Siegel, G.; Prestgard, M.C.; Teng, S.; Tiwari, A. Robust longitudinal spin-Seebeck effect in Bi-YIG thin films. *Sci. Rep.* **2014**, *4*, 4429.
146. D'yakonov, M.I. Introduction to spin physics in semiconductors. *Physica E* **2006**, *35*, 246–250.
147. D'yakonov, M.I.; Perel, V.I. Possibility of Orienting Electron Spins with Current. *JETP Lett.* **1971**, *13*, 467–469.
148. Litvinenko, K.L.; Leontiadou, M.A.; Li, J.; Clowes, S.K.; Emeny, M.T.; Ashley, T.; Pidgeon, C.R.; Cohen, L.F.; Murdin, B.N. Strong dependence of spin dynamics on the orientation of an external magnetic field for InSb and InAs. *Appl. Phys. Lett.* **2010**, *96*, 111107.
149. Saikin, S.; Shen, M.; Cheng, M.C. Spin dynamics in a compound semiconductor spintronic structure with a Schottky barrier. *J. Phys. Condens. Matter* **2006**, *18*, 1535–1544.
150. Tong, H.; Wu, M.W. Multivalley spin relaxation in n-type bulk GaAs in the presence of high electric fields. *Phys. Rev. B* **2012**, *85*, 075203.
151. Fu, J.Y.; Weng, M.Q.; Wu, M.W. Spin-orbit coupling in bulk GaAs. *Physica E* **2008**, *40*, 2890–2893.
152. Slichter, C.P. *Principles of Magnetic Resonance*; Lotsch, H.K.V., Ed.; Springer: Berlin, Germany, 1996; p. 399
153. Glazov, M.M.; Ivchenko, E.L. Precession spin relaxation mechanism caused by frequent electron-electron collisions. *JETP Lett.* **2002**, *75*, 403–405.
154. Adorno, D.P. Polarization of the radiation emitted in GaAs semiconductors driven by far-infrared fields. *Laser Phys.* **2010**, *20*, 1061–1067 .
155. Adorno, D.P.; Pizzolato, N.; Fazio, C. Elucidating the electron transport in semiconductors via Monte Carlo simulations: An inquiry-driven learning path for engineering undergraduates. *Eur. J. Phys.* **2015**, *36*, 055017.
156. Spezia, S.; Adorno, D.P.; Pizzolato, N.; Spagnolo, B. Relaxation of electron spin during high-field transport in GaAs bulk. *J. Stat. Mech. Theory Exp.* **2010**, doi:10.1088/1742-5468/2010/11/P11033.
157. Spezia, S.; Adorno, D.P.; Pizzolato, N.; Spagnolo, B. Temperature dependence of spin depolarization of drifting electrons in n-type GaAs bulk. *Acta Phys. Pol. B* **2010**, *41*, 1171–1180.
158. Adorno, D.P.; Zarcone, M.; Ferrante, G. Far-infrared harmonic generation in semiconductors: A Monte Carlo simulation. *Laser Phys.* **2000**, *10*, 310–315.
159. Peschke, C. The impact of electron-electron interaction on electron transport in GaAs at high electric fields. *J. Phys. Condens. Matter* **1994**, *6*, 7027–7044.
160. Moško, M.; Mošková, A. Ensemble Monte Carlo simulation of electron-electron scattering: Improvements of conventional methods. *Phys. Rev. B* **1991**, *44*, 10794–10803.
161. Mošková, A.; Moško, M. Exchange carrier-carrier scattering of photoexcited spin-polarized carriers in GaAs quantum wells: Monte Carlo study. *Phys. Rev. B* **1994**, *49*, 7443–7452.
162. Bena, I. Dichotomous Markov Noise: Exact Results for Out-of-Equilibrium Systems. *Int. J. Mod. Phys. B* **2006**, *20*, 2825–2888.
163. Barik, D.; Ghosh, P.K.; Ray, D.S. Langevin dynamics with dichotomous noise; direct simulation and applications. *J. Stat. Mech. Theory Exp.* **2006**, doi:10.1088/1742-5468/2006/03/P03010.
164. Shit, A.; Chattopadhyay, S.; Chaudhuri, J.R. Taming the escape dynamics of nonadiabatic time-periodically driven quantum dissipative system within the frame of Wigner formalism. *Chem. Phys.* **2014**, *431–432*, 26–38.
165. Shit, A.; Chattopadhyay, S.; Chaudhuri, J.R. Quantum stochastic dynamics in the presence of a time-periodic rapidly oscillating potential: Nonadiabatic escape rate. *J. Phys. Chem. A* **2013**, *117*, 8576–8590.
166. Devoret, M.H.; Schoelkopf, R.J. Superconducting Circuits for Quantum Information: An Outlook. *Science* **2013**, *339*, 1169–1174.
167. You, J.Q.; Nori, F. Atomic physics and quantum optics using superconducting circuits. *Nature* **2011**, *474*, 589–597.
168. Leuenberger, M.N.; Loss, D. Quantum computing in molecular magnets. *Nature* **2001**, *410*, 789–793.

169. Harris, D.O.; Engerholm, G.G.; Gwinn, W.D. Calculation of Matrix Elements for One-Dimensional Quantum-Mechanical Problems and the Application to Anharmonic Oscillators. *J. Chem. Phys.* **1965**, *43*, 1515–1517.
170. Light, J.C.; Carrington, T. Discrete-Variable Representations and their Utilization. In *Advances in Chemical Physics*; John Wiley & Sons, Inc.: New York, NY, USA, 2007; Vol. 114; pp. 263–310.
171. Magazzù, L.; Valenti, D.; Spagnolo, B.; Grifoni, M. Dissipative dynamics in a quantum bistable system: Crossover from weak to strong damping. *Phys. Rev. E* **2015**, *92*, 032123.
172. Thorwart, M.; Grifoni, M.; Hänggi, P. Strong Coupling Theory for Driven Tunneling and Vibrational Relaxation. *Phys. Rev. Lett.* **2000**, *85*, 860–863.
173. Grabert, H.; Schramm, P.; Ingold, G.L. Quantum Brownian motion: The functional integral approach. *Phys. Rep.* **1988**, *168*, 115–207.
174. Leggett, A.J.; Chakravarty, S.; Dorsey, A.T.; Fisher, M.P.A.; Garg, A.; Zwerger, W. Dynamics of the dissipative two-state system. *Rev. Mod. Phys.* **1987**, *59*, 1–85, doi:10.1103/RevModPhys.59.1.